
Technical Letter Report on Development of Flaw Sizing Algorithms for Eddy Current Rotating Probe Examinations

September 2008

Prepared by
Sasan Bakhtiari and Thomas W. Elmer

Argonne National Laboratory
9700 South Cass Avenue
Argonne, IL 60439

M. Stambaugh, NRC Project Manager

Prepared for
Division of Engineering
Office of Nuclear Regulatory Research
U.S. Nuclear Regulatory Commission
Washington, DC 20555-0001
NRC Job Code N6583



Contents

Contents	ii
List of Figures	iii
Acknowledgments.....	viii
Executive Summary.....	ix
Acronyms and Abbreviations.....	x
I. Introduction.....	1
II. Background	3
III. Objectives	5
IV. Structure of Data Analysis Tool	6
IV.1 Conversion Process	7
IV.2 Calibration Process	9
IV.3 Data Analysis Tools.....	13
IV.3.1 Measurement Routines	14
IV.3.2 Filter Routines.....	16
IV.3.3 Flaw Sizing Algorithms.....	20
IV.3.4 Scripting Tool	23
IV.3.5 Incorporation of User-developed Algorithms.....	25
IV.3.6 Exporting of Data.....	27
V. Test Case Results on Flaw Sizing.....	29
VI. Summary.....	47
References.....	48

List of Figures

1. Representative display of different stages of data conversion process performed directly from the main GUI. Shown here are the converted data acquired with a rotating probe. The file import dialog box with the list of recognized file types is shown on the right. The image panels of the GUI on the left display the (top) trigger channel that was detected automatically and (bottom) raw data from another channel showing two calibration standard tubes. 8
2. Representative display of different stages of data calibration process performed directly from the main GUI. Initial loading of rotating probe data from two calibration standard tubes is displayed in Fig. 2(a). Also shown on this figure is the dialog box for selection of the process channels to append to the original channel list. Segmented and calibrated data is displayed in Fig. 2(b). The Channels pull-down menu shows the added process channels (marked on the menu). Data displayed in the image panels are the 300 kHz (top) axial and (bottom) circumferential channel. 11
3. Calibration curves generated simultaneously for all rotating probe channels from the GUI. Shown here are the phase-based depth curves for (a) +Point™ and (b) mid-range pancake coil at 400 kHz, 300 kHz, 200 kHz, and 100 kHz frequencies. The input values used for generating the curve are marked on each plot..... 12
4. Data analysis tools available under different menus of the GUI. Shown here are the expanded views of current list of functions under four pull-down menus. 13
5. Representative graphics associated with the use of functions under the measurement menu. Shown here are (a) manual measurement of signal amplitude and phase based on peak-to-peak and maximum rate of change and (b) automated measurement of flaw signals over the same data segment from a calibration standard tube. The data segment displayed in the GUI includes a 60% TW and an 80% TW axial EDM notch detected with a +Point™ probe at 300 kHz. 15
6. An example of data superposition tool used to simulate the effect of closely spaced signals and nearby artifacts on the probe response. The data segment used for demonstration is the portion of the calibration standard tube covering four OD axial EDM notches ranging from 20%TW to 80%TW and the simulated TSP collar. Displayed here are the +Point™ probe response at 300 kHz for (a) the original and (b) manipulated data with the 60% TW flaw signal inserted near the 80% TW flaw and at the edge of the TSP. 18
7. An example of data superposition tool used to insert rotating probe data from a 360° section of one tube into another tube. Graphics show (a) calibrated EC inspection data from a mock-up tube with multiple indications at a dented TSP region, and (b) the same tube with a second TSP section superimposed on it (near tube end on the right hand side). The superposition was simultaneously applied to all the test channels. Data displayed in the analysis window pertains to the +Point™ probe at 300 kHz frequency..... 19

8. Illustration of the segmentation process for two algorithms evaluated to determine the optimal approach for processing of EC inspection data over the entire length of tube. Threshold-based initial segmentation of data with five ROIs is illustrated in Fig. 8(a). The following drawings in Figs. 8(b) and (c) illustrate two possible outcomes for linking of the small patches of data with no relevant signals, marked as A and B, to their neighboring ROIs. While the segmentation shown in Fig. 8(b) often results in a more uniform distribution of ROIs, it can lead to their improper linkage resulting in potential gaps. The result based on the second algorithm that assumes helically scanned data is more correlated along the circumferential direction is illustrated in Fig. 8(c). The process in this case is more computationally efficient and has proven to be more robust in linking of ROIs. 21
9. An example of generating a script file using the function available under the *Scripts* menu of the GUI. Shown here are (a) identifier 'keys' marked on the bottom right corner of the analysis window for the set of processes applied to data and (b) the script file generated automatically from the *Scripts* menu containing a list of all the processes and their associated arguments. Functions in the sample script here include the pre-processing, rule-based identification, signal detection, and depth sizing routines. The scripting option allows a sequence of user-selected processes to be automatically applied to the data. 24
10. A simple example for creating and executing a filter routine under the new GUI plugin system. Displayed here are (top) text of a file for a simple filter routine that was generated for demonstration purposes, (middle) inclusion of the new filter name as the first item under the *Filters* menu following refreshing of the list and display of the multi-character filter 'key' at the bottom the analysis window following its application, and (bottom) result of the operation on data displayed in the command window. 26
11. Representative ExcelTM plots generated from the output of data analysis GUI. A script has been implemented that allows exporting of the final sizing results into text format. Results shown here are exported sizing results for indications in two mock-up test sections with (a) multiple and (b) single OD axial crack that are part of the data set selected for studies associated with the equivalent rectangular crack model. 28
12. Display of data at various stages of the process for sizing of and an ID initiated indication in a mock-up TSP test section. Graphics show (a) the +PointTM data for the entire tube section at 300 kHz in various display formats, (b) filtered data after suppression of the TSP signal, (c) filtered data over a short section covering the flawed region of the tube, (d) the sizing results displayed in a separate window and with amplitude and depth profiles displayed in cross sectional plot and in image format. The results in this case indicate presence of a ~1-in.-long ID crack with a maximum depth of slightly deeper than 80% TW..... 30
13. Display of data at various stages of the process for sizing of and an OD initiated indication in a mock-up free-span test section. Graphics show (a) the +PointTM data for the entire tube section at 300 kHz in various display formats, (b) filtered data after suppression of the TSP signal, (c) filtered data over a short section covering the flawed region of the tube, (d) the sizing results displayed in a

- separate window and with amplitude and depth profiles displayed in cross sectional plot and in image format. The results in this case indicate presence of a >1-in.-long OD crack with a maximum depth of >90% TW..... 31
14. Display of data at various stages of the process for sizing of OD initiated multiple axial indications in a mock-up tube section. Graphics show (a) the +Point™ data for the entire tube section at 300 kHz in various display formats, (b) filtered data over a short section covering the flawed region of the tube, and (c) axial and (d) circumferential profile of the flawed region. The sizing results are displayed in a separate window with amplitude and depth profiles displayed in cross sectional plot and in image format. The results in this case indicate presence of two nearly parallel axial cracks of different lengths that are <50° apart circumferentially. Axial profile of the longer (~0.5 in.) crack displayed in Fig. 14(c) shows a maximum depth of >90% TW. The circumferential profile shown in Fig. 14(d) suggests the maximum depth of the shorter crack (~0.25 in.) to be >80% TW. 34
 15. Display of data at various stages of the process for sizing of OD initiated axial indication in a mock-up tube section. Graphics show (a) the +Point™ data for the entire tube section at 300 kHz in various display formats, (b) filtered data after suppression of the TSP signal over a short section covering the flawed region of the tube, and (c) the sizing results displayed in a separate window and with amplitude and depth profiles displayed in cross sectional plot and in image format. The results in this case indicate presence of a ~0.2-in.-long axial crack with a maximum depth of ~90% TW. 35
 16. Display of data at various stages of the process for sizing of OD initiated circumferential indication in a mock-up tube section. Graphics show (a) the +Point™ data for the entire tube section at 300 kHz in various display formats, (b) filtered data over a short section covering the flawed region of the tube, and (c) the sizing results displayed in a separate window and with amplitude and depth profiles displayed in cross sectional plot and in image format. The results in this case indicate presence of >200° circumferential cracking with a maximum depth of ~70% TW. 36
 17. Data displayed at various stages of the process for sizing of indications at a dented TSP region in a mock-up tube section. Graphics show (a) the calibrated +Point™ data for the entire tube section at 300 kHz in various display formats, (b) filtered data over a short section covering the flawed region of the tube, and (c) the sizing results displayed in a separate window and with amplitude and depth profiles displayed in cross sectional plot and in image format. The results in this case indicate presence of multiple OD axial indications with the longer indication having a length of >1-in. with an average depth of ~60%TW and a maximum depth of <70% TW..... 37
 18. Data displayed at various stages of the process for sizing of indications at a dented TSP region in a mock-up tube section. Graphics show (a) the calibrated +Point™ data for the entire tube section at 300 kHz in various display formats, (b) filtered data over a short section covering the flawed region of the tube, and (c) the sizing results displayed in a separate window and with amplitude and depth profiles displayed in cross sectional plot and in image format. The results

	in this case indicate presence of multiple OD axial indications with the longer indication having a length of <1-in. and a maximum depth of ~70% TW.	38
19.	Data displayed at various stages of the process for sizing of indications at a dented free-span region in a mock-up tube section. Graphics show (a) the calibrated +Point™ data for the entire tube section at 300 kHz in various display formats, (b) filtered data over a short section covering the flawed region of the tube, and (c) the sizing results displayed in a separate window and with amplitude and depth profiles displayed in cross sectional plot and in image format. The results in this case indicate presence of multiple OD axial indications with the longer indication having a length of >0.25-in. and a maximum depth of <70% TW.....	39
20.	Example of superposition of EC inspection data collected from two separate tube sections. Simulated data here was generated to demonstrate sizing of indications over the entire length of tube. Graphics show (a) raw data from a tube section with multiple indications at a dented TSP region, and (b) the same tube with superimposed flaw signals. The same free-span SCC signal was inserted into three locations, one in the free-span region and two in the TSP region (center and edge), that are delineated on the image display. Eddy current inspection data displayed in the analysis window is from +Point™ probe at 300 kHz.....	42
21.	Data displayed at different stages of the process for sizing of indications in the simulated test section shown in Fig. 20(b). Graphics show (a) detected indications over the entire tube after elimination of background signals and (b) the depth sizing results over the entire length of the tube displayed in the main GUI. The results in this case indicate that in addition to the original signals in the TSP region of the tube, all three simulated flaw signals were also detected and sized.....	43
22.	Data analysis results over three small segments covering the superimposed SCC signals of Fig. 21(b) located in free-span and TSP region of the tube. Graphics show the amplitude and depth profiles of the same indication based on the processed +Point™ data at the (a) free-span region, (b) center of TSP, and (c) the edge of TSP. The profiles for all three locations show good agreement among the sizing results.	44
23.	Display of the EC rotating probe data at different stages of the process for a tube section with multiple axial indications at a dented TSP region. Graphics show the +Point™ data at 300 kHz (a) after the calibration stage and (b) following the pre-processing, detection, and rule-based identification stage. The processed data suggest presence of multiple OD-initiated axial indications around the tube's circumference.	45
24.	Flaw sizing results for the rotating probe data shown in Fig. 23. Shown here in the main GUI are the estimated depth values based on a single frequency (a) over the entire tube and (b) over a small region covering the dominant TSP indication. Also shown are the single and multiple frequency sizing data for the same region of the tube as in Fig. 24(b) using the phase information from (c) 300 kHz, (d) 400 and 300 kHz, and (e) 400, 300, and 200 kHz channels. The estimated depth	

profiles for the dominant flaw suggest close agreement between the three sizing results. 46

Acknowledgments

This work is sponsored by the Office of Nuclear Regulatory Research, U.S. Nuclear Regulatory Commission (NRC), under Job Code N6583. The NRC Project Manager is Margaret Stambaugh.

Executive Summary

Manual analysis of multiple-frequency eddy current (EC) data, either for detection or for sizing of flaws, is a tedious and challenging process. Conventional data analysis methods become rather subjective when dealing with complex forms of degradation such as stress corrosion cracking. Signal distortion by interference from internal or external artifacts in the vicinity of a flaw further complicates discrimination of flaw signals from noise. Proper application of signal processing and data analysis techniques can help reduce the influence of noise and consequently improve the signal-to-noise ratio. Computer-aided data analysis tools that employ such algorithms can increase the detection capability and the consistency of sizing results among analysts. Furthermore, software-based tools can significantly increase the process efficiency that is needed for more routine application of detailed sizing procedures during field inspections.

This report provides an overview of research activities at Argonne National Laboratory (ANL) associated with computer-aided analysis of EC inspection data. The overall objective of the studies in this area has been to examine viable methods that could help improve the reliability of tube integrity assessments based on nondestructive evaluation (NDE) results. The NDE results were used both to assess the capability of a particular EC inspection method for sizing of flaws and as input to mechanistic models for prediction of the structural integrity of SG tubes. The structural integrity evaluations are presented in a separate report. The results of efforts on the development and integration of various algorithms for sizing of flaws based on eddy current rotating probe data are presented here. The main focus of these investigations was on the processing of data acquired with the +Point™ probe, which is one of the more widely used probes for detection and characterization of cracking in SG tubes. It should be noted, however, that many of the processes described in this report are applicable to data acquired with other probe types and under different test conditions. The overall structure of a software-based tool, developed under the MATLAB® environment, for the processing of data acquired with different EC probe types is described in this report. The three major stages of the process that have been consolidated under a single graphical user interface are discussed. The main algorithms for sizing of flaws are also described. Representative cases are provided that illustrate the processes involved in generating the final estimate of the flaw size. The examples further demonstrate the options available for the processing of data over a selected region or the entire length of the tube. Other functions including those implemented for superposition of data and for exporting of data in standard formats are also described.

Acronyms and Abbreviations

ANL	Argonne National Laboratory
ASME	American Society of Mechanical Engineers
EC	Eddy Current
EDM	Electro-discharge-machined
GUI	Graphical User Interface
ID	Inside Diameter
ISI	Inservice Inspection
RPC	Rotating Probe Coil
NDE	Nondestructive Evaluation
NRC	Nuclear Regulatory Commission
OD	Outside Diameter
ROI	Region of Interest
SCC	Stress Corrosion Cracking
SG	Steam Generator
S/N	signal-to-noise ratio
TS	Tube-sheet
TSP	Tube Support Plate
TW	Throughwall
UID	Unique identifier

I. Introduction

Reliable detection and characterization of flaws in steam generator (SG) tubes is important for the evaluation of tube structural integrity. Eddy current (EC) testing in its various forms is the primary method for in-service inspection (ISI) of SG tubes. High-speed bobbin probes are used for full-length inspection of the SG tube bundle. Intrinsic to its coil design, bobbin probe provides a single circumferentially integrated measurement at each position along the tube axis. The relatively large coverage of the coil also limits its ability to resolve closely spaced discontinuities along the tube axis. Motorized rotating probe coils (MRPC) are routinely employed for more detailed examination of selected regions of the SG tube (e.g., tube sheet, support plates, and U-bend region) or as a supplementary technique for confirmation of signals detected initially by bobbin probes. Rotating probes traverse the tube with a helical motion that results in a complete scan of the tube wall. The probe head assembly may contain single or multiple surface coils that can provide complementary information. Both impedance and transmit-receive probe configurations are available. Directionally sensitive probes are used to more decisively identify the orientation of crack-like indications. The coils may be excited in either absolute or differential mode. One common surface-riding rotating probe design in use today consists of three coils that are integrated into a single probe head: a differential cross wound coil (referred to as +Point™), an absolute mid-frequency pancake coil, and an absolute high-frequency pancake coil. Because MRPCs in general offer the highest spatial resolution among all eddy current probe types used for field applications, they are often employed to ultimately resolve and size potential flaws. Conventional procedures for estimation of flaw size, either for ISI applications or for subsequent engineering assessments, are based primarily on manual analysis of rotating probe data. The process for generating depth profiles in this manner is rather tedious and the results are subject to variability among analysts. Development of computer-aided data analysis tools is a viable approach to help improve the reliability, repeatability, and efficiency of flaw sizing based on rotating probe examinations.

This report provides an overview of research activities at Argonne National Laboratory (ANL) associated with computer-aided analysis of EC inspection data. The overall objective of the studies in this area has been to examine viable methods that could help improve the reliability of tube integrity assessments based on the nondestructive evaluation (NDE) results. The NDE results were used both to assess the capability of a particular EC inspection method for sizing of flaws and as input to mechanistic models for prediction of the structural integrity of SG tubes. The results of structural integrity evaluations are presented in a separate report. The results of efforts on the development and integration of various algorithms for sizing of flaws based on eddy current rotating probe data are presented here. The main focus of these investigations was on the processing of data acquired with the +Point™ probe, which is one of the more widely used surface probes for detection and characterization of cracking in SG tubes. It should be noted, however, that many of the processes described in this report are applicable to data acquired with other probe types and under different test conditions.

In the following sections, the overall structure of a software-based tool, developed under the MATLAB® environment, for the processing of data acquired with different EC probe types is initially described. The three major stages of the process that have been consolidated under a single graphical user interface (GUI) are subsequently discussed. They are referred to as the conversion, calibration, and the analysis stage. The main algorithms for sizing of flaws are described as part of the data analysis stage. Representative cases are provided that illustrate the processes involved in generating the final estimate of the flaw size. The examples further demonstrate the options

available for the processing of data over a selected region or the entire length of the tube. Other functions including those implemented for superposition of data and for exporting of data in standard formats are also described.

II. Background

Manual analysis of multiple-frequency eddy current (EC) data, either for detection or for sizing of flaws, is a tedious and challenging process. Conventional data analysis methods become rather subjective when dealing with complex forms of degradation such as stress corrosion cracking (SCC). Signal distortion by interference from internal or external artifacts in the vicinity of a flaw further complicates discrimination of flaw signals from noise (any unwanted signal). Separate studies associated with nondestructive evaluation (NDE) of SG tubing performed at ANL demonstrated that EC noise in general has a more profound effect on the estimation of the flaw size than it does on the ability to detect a flaw signal.¹ Other studies involving manual estimation of the depth profile for SCC type flaws in laboratory-degraded specimens also indicated that significant variability could exist among the sizing results by different analysts, particularly when dealing with weak signals.^{2,3} Software-based signal processing and data analysis techniques, when applied properly, can help reduce the influence of noise and consequently improve the signal-to-noise ratio (S/N). Computer-aided data analysis tools that employ such algorithms can increase the detection capability and the consistency of sizing results among analysts. Furthermore, software-based tools can significantly increase the process efficiency that is needed for more routine application of detailed sizing procedures during field inspections.

Previous research activities at ANL on improved inservice inspection (ISI) technology for steam generator (SG) tubes focused in part on the assessment of viable signal processing and data analysis methods for EC probes. As part of that work, various software-based tools were developed to allow independent analysis of EC data collected with standard commercial test equipment. A number of separate routines, all implemented in MATLAB[®] programming language, were developed over time for conversion, calibration, and analysis of data collected with different probe types. A detailed description of that work has been presented in a number of earlier reports.⁴⁻⁷

Latest research activities on computer-aided analysis of EC inspection data focused in part on consolidation of the various routines that perform different stages of data manipulation under a common graphical user interface (GUI). A major goal of this undertaking was to develop a more user-friendly research tool that would allow more efficient implementation and testing of new signal processing and data analysis algorithms. A MATLAB[®]-based user interface has been developed for this purpose. The modular structure of the GUI allows user-developed routines to be easily incorporated, modified, and tested independent of the core code. The software can be used for either manual or automated analysis of data. The measurement and visualization tools currently embedded in the GUI allow the data to be manually examined at any stage of the process. Furthermore, access to both the original and the processed data permits direct comparison of the data before and after application of a particular algorithm. Data at any stage may also be exported in a standard format for further manipulation outside the MATLAB[®] environment. Various other functions including those for measurement of noise and for superimposing of signals have also been integrated into the GUI.

Rotating probes in general provide the highest spatial resolution among all EC probe types and thus are employed for more detailed examination of selected regions of SG tubes. The +Point[™] probe, which has an orthogonally-wound differential coil configuration, is currently one of the more prominent rotating probes used by the industry for detection and characterization of crack-like indications in SG tubes. Data collected with the +Point[™] probe is routinely used for estimation of the flaw size during field applications. The sizing procedure commonly involves manual measurement of the depth, primarily based on the phase angle of the signal, along the length of the

flaw. A depth profile is generated by recording of the measurements for a number of points on both sides of the peak amplitude response from the flaw. Because rotating probes generate significant amount of data, the profiling of flaw depth is often performed on a selective basis and often as part of engineering assessments. As the main focus of this work, efforts were undertaken to extend the computer-aided data analysis techniques developed for rotating probe data so that they can be used to analyze data acquired with the +Point™ probe. A new data analysis GUI was developed under this program and has been used to test the algorithms for sizing of flaws based on +Point™ data. Functionality is provided under the GUI to automatically generate the flaw size over a selected region or over the entire length of a tube. New routines have also been incorporated to allow estimation of flaw depth based on alternative methods. The algorithms provide different degrees of conservatism in estimating of the flaw size. The NDE sizing data generated under this program also served as input to mechanistic models for the prediction of tube structural integrity that was studied under a separate task. The results of those studies will be published in a separate report.⁸

III. Objectives

The overall objective of studies on computer-aided analysis of eddy current (EC) inspection data at ANL has been to examine viable methods that could help improve the reliability of tube integrity assessments based on the nondestructive evaluation (NDE) results. Various algorithms have been developed for manipulation of NDE data collected with prominent EC probes used for field applications. Specific objectives of this work were a) develop and consolidate the algorithms for sizing of flaws for use under a software-based data analysis tool, and b) provide NDE estimate of flaw size as input to mechanistic models for prediction of tube structural integrity that is being studied under a separate task. The main focus of the efforts was on the processing of data acquired with the +Point™ rotating probe, which is one of the more widely used probes for detection and characterization of cracking in SG tubes. It is expected, however, that many of the processes described in this report are applicable to data acquired with other probe types and under different test conditions.

IV. Structure of Data Analysis Tool

The general structure of a computer-aided data analysis tool for the processing of EC inspection data is described next. As part of earlier studies in this area, various stand-alone routines were developed to allow independent manipulation of data collected with different EC probe types used during field examinations. Separate user interfaces, all implemented using MATLAB[®] programming language, were developed to perform conversion, calibration, and analysis of EC inspection data. As part of the more recent efforts, these separate stages of data manipulation have been consolidated under a common graphical user interface (GUI). Previously developed algorithms have been updated and made compatible to run under the new software structure. The algorithms for sizing of flaws have been integrated into the GUI for analyzing of data acquired with rotating probes. The focus of these efforts was on the analysis of data collected with the +Point[™] probe. More functionality has been added in terms of the user's ability to examine data at any stage of the process. This research tool can be used for both manual and automated analysis of EC inspection data.

The data analysis GUI was created in order to facilitate testing of routines dynamically without the need for reloading of data or repeating of the previous steps each time a change is made to an intermediate process. The user interface abstracts certain parts of the data processing and management, thus allowing a routine to be implemented without a detailed knowledge about the structure and handling of the data. For example, the cross-section of data currently displayed in the image panels may be retrieved by simply calling the associated function without the need to specify the channel number or the location of points in the data matrix. Similarly, information about any data point (i.e., position, amplitude, phase, and depth) is instantaneously displayed by clicking on the display panel. The embedded graphical tools of the user interface allow for extended zooming and scrolling of data for more detailed manual analysis. Data may be visualized in one-, two-, or three-dimensional display formats as well as in strip-chart and Lissajous (impedance plane) plots. The display options can be further extended by incorporating other custom plots. To further assist in evaluating of algorithms, the processed data may readily be compared with the original data or with data from other test channels at any stage. Also, the action of a routine can always be reverted and the operation may be reapplied following modifications. The order in which the processing steps are applied can be easily modified and re-tested. The above actions may all be performed without the need to reload the data or repeating of the previous stages of data analysis. Processed data can be saved at any point during the analysis stage. This eliminates the need for repeating of previous operations when the same data is to be further manipulated at a later date. Finally, the data analysis steps can be saved into a script file and can be applied to another data file with minimal user intervention. The ability to create a MATLAB[®] subroutine (plugin) with less focus on the handling of data permits more efficient implementation and evaluation of new routines under the GUI.

As noted above, the GUI was built around the various codes developed over time to independently analyze EC inspection data. The most notable feature of the software is its plugin structure that facilitates more convenient implementation and testing of new user-developed routines. Its modular user interface allows functions to be manipulated independent of the main code, thus making it more immune to process errors. New plugins (i.e., MATLAB[®] routines with specific header information) can be linked to the GUI by simply including the specified header information and placing the file in the appropriate directory. Improvements have also been made with regard to file validation and error checking, which are performed when a data file is initially loaded and when the functions are executed, respectively. More functionality has also been

provided with regard to importing and exporting of data. Under the new GUI, importing of raw EC inspection data is carried out in a more transparent manner (i.e., minimal user interaction). Exporting of data into a standard file format for manipulation outside the MATLAB® environment can be done at any stage of the process following the calibration stage. Another important feature of the updated user interface is its scripting tool, which permits sequential application of multiple operations in an automated manner. This capability allows for efficient processing of a large number of data files that are to be analyzed using the same set of processes.

With the new plugin system, user-defined routines may be linked under the measurement, filters, and scripting menus. The functions under the *Measure* menu provide several standard options for the measurement of signal amplitude and phase along any arbitrary cross section of the tube. The functions under the *Filters* menu modify the data. They include, among other routines, various spatial and frequency domain signal processing algorithms intended primarily for improving of the signal-to-noise ratio (S/N) by reducing the level of background noise and suppressing of artifacts. The functions under the *Scripts* menu are used to automatically generate and execute script files containing a list of user-defined processes. Although no menus are provided, plugin routines can also be incorporated in a similar manner into certain other directories such as those associated with the calibration and file handling, which was not previously attainable. Help menus have been assembled that describe the procedure for creating a plugin routine. The help menu also provides a general description of the structure of the GUI as well as documentation on the associated functions and variables.

The flaw sizing algorithms here refer to a number of signal processing and data analysis routines that have been assembled under the *Filters* menu of the GUI. These filters are applied to the EC inspection data to ultimately generate the final estimate of flaw size in a tube. Various routines developed earlier for the manipulation of data acquired with rotating probes have been refined and integrated into the GUI. These routines have been adapted for use with the new plugin system. With the focus of recent studies being on the +Point™ rotating probe, additional data handling capabilities have been incorporated in order to more effectively deal with data collected with that particular probe. Because of the bipolar nature of the +Point™ coil response, it is more convenient to establish separate channels for the examination of signals from discontinuities with axial and circumferential orientation. A number of examples on the analysis of +Point™ data are provided in the following sections.

IV.1 Conversion Process

Raw data acquired with a commercial EC instrument must be first converted to a MATLAB® readable format before it can be further manipulated with the data analysis tool. Description of the conversion and segmentation routines developed earlier at ANL has been provided in other reports.⁶ In brief, the file header information is first read in order to retrieve the minimum necessary information regarding the type of data, the number of channels, and the test frequencies used for inspection of the SG tube. Based on that information the original data is subsequently parsed, read, and converted into proper format for further manipulation with the data analysis tool. Formerly, the conversion and initial segmentation of data was performed by a separate interactive program. The process relied on the user to provide a number of inputs including the type of EC test instrument and probe for proper conversion of the raw data. To eliminate the need for executing separate set of programs for each stage of the process and to further reduce analyst intervention, a more versatile programming structure had to be implemented. The new plugin structure allowed the independently developed routines to be integrated under one user interface.

Data conversion plugins have been created for use under the new data analysis GUI. The new software structure further allowed implementation of algorithms for importing of other types of data that was not previously attainable. Raw EC inspection data can now be imported directly from the main user interface. New algorithms have also been developed that automatically detect the trigger channel for rotating probes during the file conversion process. A dialog box has been added which permits loading of several different file types. Data file recognition is based in part on the file's extension and the conversion process is carried out in a semitransparent manner. The file types that are currently recognized include those acquired with certain commercial EC test equipment (e.g., Miz-18, Miz-30 and Miz-70 from Zetec, Inc.) as well as text, Excel™, and LabView™ files. New scripts may be added in the future for recognition of other types of data file. As part of the data conversion process, the option is provided to select and save an arbitrary length of data. Upon completion of the conversion process the data is automatically saved in the current directory with the same filename but with a different file extension to indicate that the file has been processed. A separate text file is also created at this stage that contains the header information associated with the number of channels and test frequencies. Data at this initial stage can be segmented and the channels can be down-selected in order to reduce the amount of data carried through the following stages. During the initial stage, data can be segmented, rotated, and specific channels can be chosen to reduce the amount of data carried through the following stages. Further segmentation of data may be performed each time a file is first loaded by the GUI.

An example of data imported directly from the main GUI and its conversion to a format appropriate for manipulation with the data analysis tool is provided in Fig. 1. The graphics show raw EC inspection data collected with a rotating probe on a pair of in-line tubes consisting of an

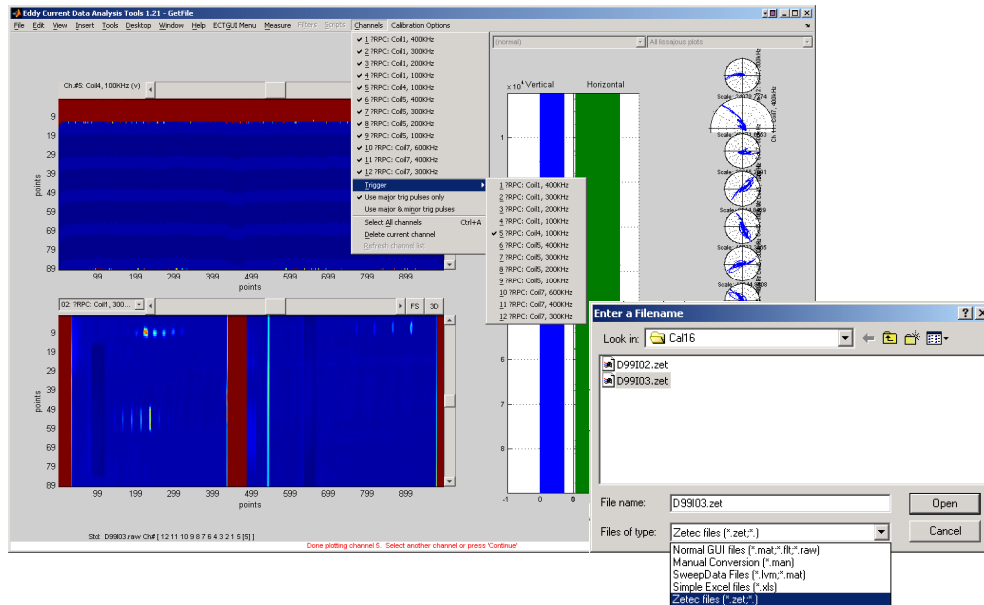


Figure 1. Representative display of different stages of data conversion process performed directly from the main GUI. Shown here are the converted data acquired with a rotating probe. The file import dialog box with the list of recognized file types is shown on the right. The image panels of the GUI on the left display the (top) trigger channel that was detected automatically and (bottom) raw data from another channel showing two calibration standard tubes.

EDM notch and an ASME calibration standard. As shown in Fig. 1, the file import dialog box with a list of recognized file types in the current directory is initially displayed. The browser can be used to import data from another directory or to search the directories for files with a different extension. The selected file, if in a recognizable format, is subsequently converted and the raw data is displayed in different graphical formats in the main GUI. The image display panels of Fig. 1 show the trigger channel in the top image panel that is composed of one major and four minor rectangular pulses. The 'Channels' pull-down menu indicates the trigger channel number that was automatically detected. The trigger channel information is used to align the helically scanned data from a tube. The raw data from a test channel is displayed in the bottom image panel, which shows the entire length of data from the two calibration standard tubes. The status of each stage of the process is indicated in the message display panel located on the bottom of the GUI. Upon completion of the conversion process, the user may continue uninterrupted to the calibration stage, which is discussed in the following section.

IV.2 Calibration Process

Uniform calibration of EC inspection data is essential for obtaining consistent data analysis results. The calibration procedure in general involves normalizing of the amplitude and adjusting of the phase angle of data based on signals from known flaws in a calibration standard tube. Algorithms developed earlier for the calibration of EC data treated bobbin (spatially one-dimensional) and rotating probe (spatially two-dimensional) data in a similar manner. This approach made it difficult to perform calibration of rotating probe based on reference standards with multiple flaws at the same axial location along the tube axis. The calibration algorithms have been refined and converted into plugin routines for integration under the new user interface. Because calibration is now performed from the main GUI, the process is better suited for handling of rotating probe data collected from different calibration standard tubes. The graphical data manipulation tools of the user interface can now be used to more precisely select and measure closely-spaced signals and the measurements can be made in either axial or circumferential direction.

Updating of the calibration routines to add new calibration steps in particular posed certain challenges. These were associated primarily with modifying of the original data structure that stored the variables from different stages of the calibration process. The new plugin system allowed implementation of more user-friendly calibration routines. Because of the modular structure of the GUI, the routines may now be modified independent of the core code thus making the process more immune to propagation of errors.

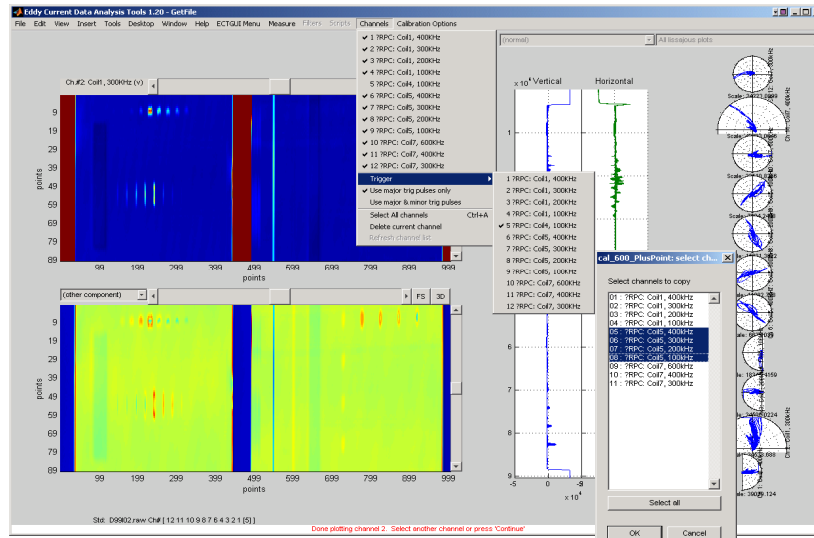
The calibration process for rotating probe data involves a number of common steps that include coil alignment, amplitude normalization, phase adjustment, and spatial scaling of data. Options to resample the data and append channels to the current list are also provided as part of the calibration process. The default for channel selection is the entire list of the available channels. Specific channels may be de-selected in order to reduce the size of data for subsequent analysis. Coil alignment is performed when more than one coil is detected from the channel configuration file. Aligning of coils allows comparison of the responses of different coils from the same location on the tube. Amplitude normalization and phase alignment are based on the signals from known flaws on a calibration standard tube. Spatial scaling of data in the axial direction is based on user-defined spacing between known indications and circumferential scaling is done based on the diameter of the tube. Selected channels may also be calibrated independently if that option is activated at the beginning of the calibration process. Re-sampling of data in either axial,

circumferential, or in both directions can be performed at the calibration stage to either increase or decrease the sample rate at which data was originally acquired. Upon completion of the calibration process, the calibration values are stored for subsequent application to other data files. When data is initially loaded, the user is prompted to either use a previously stored calibration file or continue with creating a new one. The same data may also be recalibrated at a later stage.

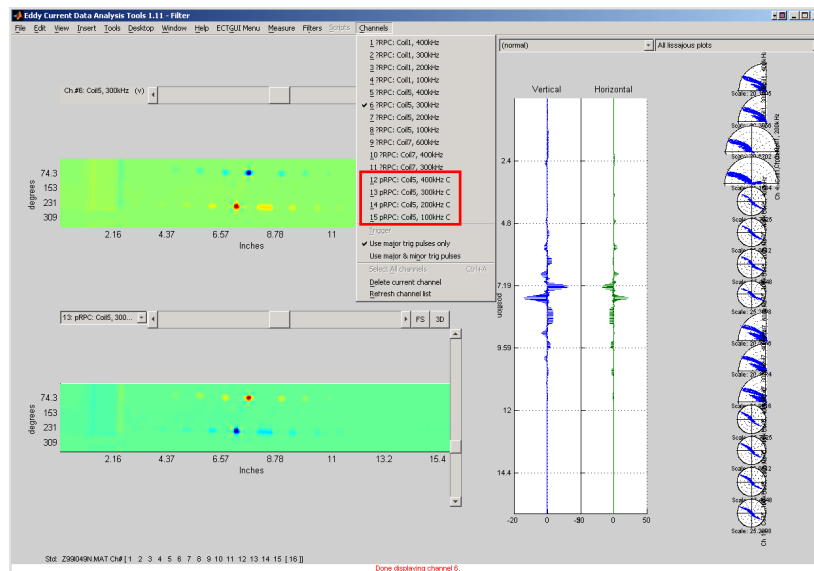
During the calibration process, selected channels may be copied, rotated, and appended to the original channel list. This option was added to specifically deal with data acquired with the +Point™ directional probe for which axial and circumferential discontinuities in a tube exhibit opposite polarity. In this way, separate channels associated with the probe's response to axial and circumferential indications could be processed individually. An example of rotating probe data calibration following the processes described above is shown in Fig. 2. Initial loading of raw EC inspection data from two in-line calibration standard tubes is displayed in Fig. 2(a). Also shown on this figure is the dialog box for selecting the channels to append to the original channel list. Figure 2(b) displays the segmented and calibrated data for one the two standards. The Channels pull-down menu shows the added process channels.

Major refinements have also been made with regard to calibration validation and error checking. Under the new plugin system, file checking is done to ensure that a loaded calibration file corresponds to the current data file being calibrated. As part of the calibration validation process, additional checks are done to ensure that the stored values corresponded to the correct calibration steps. This was done in part by assigning a unique identifier (UID) to each calibration plugin and saving the UID with the calibration file when that data is saved. When a data file is loaded for calibration, the algorithm checks whether the previously calibrated channels match with the current channels. If an exact match is found, the process will continue uninterrupted. Otherwise, the algorithms will attempt to find a “best match” between the previously calibrated and current channels and prompts for user response regarding the termination of the process or continuation using the matching channels.

Following the initial calibration stage, phase- or amplitude-based calibration curves may be generated for use by other algorithms for flaw sizing. The function called from the GUI can be used to simultaneously create calibration curves for all or a subset of channels. Signals from known manufactured flaws in a calibration standard tube are generally used for this purpose. The information provided by the user includes the origin of flaws (OD, ID, or both), the type of calibration curve (phase or amplitude), and the measurement method for the signal amplitude and phase. The selection of channel groups for which the calibration curves are automatically generated is done through dialog boxes. Following the selection of signal locations from the calibration standard tube, the curves are sequentially generated and displayed, and the calibration data is stored in a user defined file for subsequent applications. An example of phase-based calibration curves generated for the +Point™ and the mid-range pancake coil channels of a rotating probe is shown Fig. 3. Each depth-versus-phase curve in this example was generated by using a three-point piece-wise polynomial fit for the ID and the OD flaws. Interpolation through a larger number of data points could produce a more accurate calibration curve. Comparison of the two sets of curves in Figs. 3(a) and (b) shows similar trends for the +Point™ and the pancake data particularly at the higher frequencies.

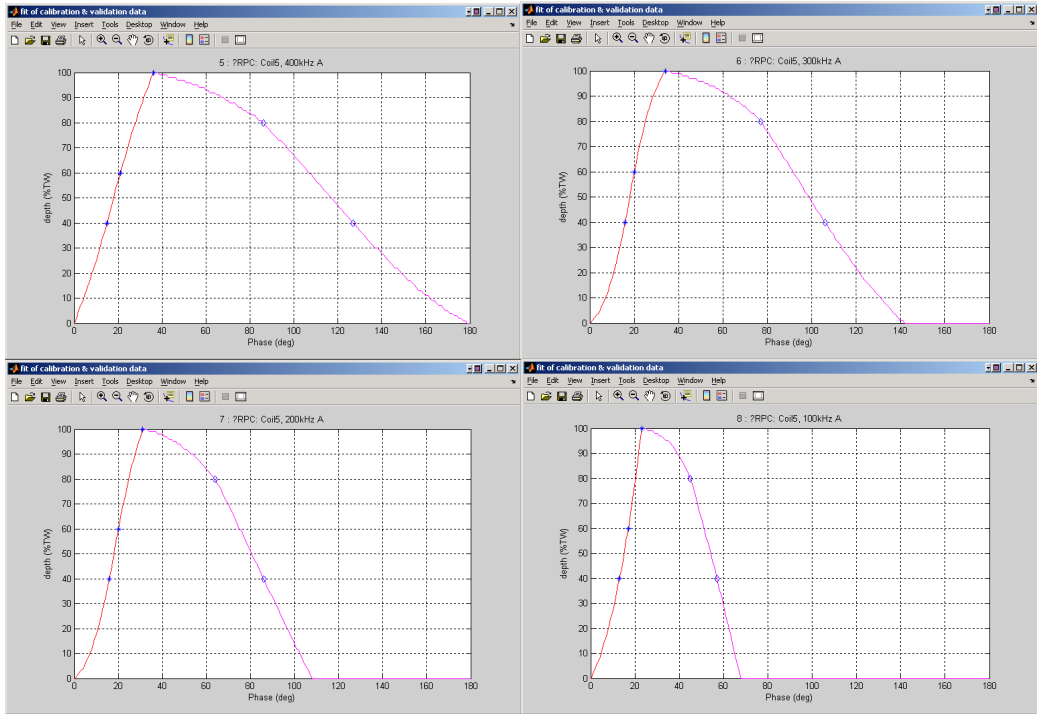


(a)

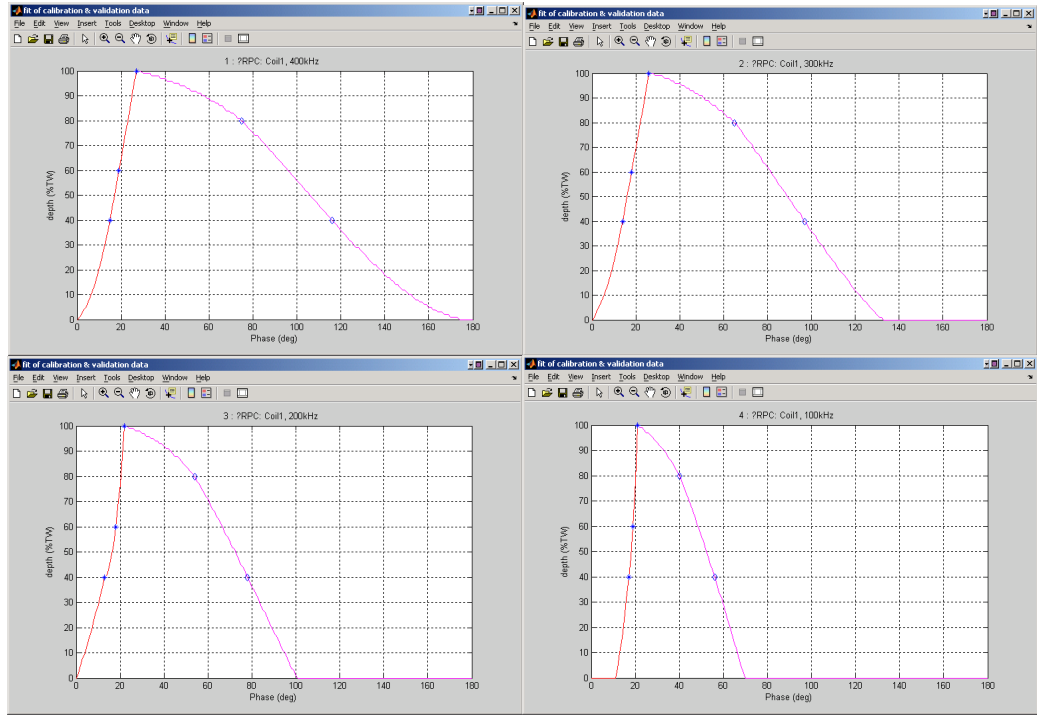


(b)

Figure 2. Representative display of different stages of data calibration process performed directly from the main GUI. Initial loading of rotating probe data from two calibration standard tubes is displayed in Fig. 2(a). Also shown on this figure is the dialog box for selection of the process channels to append to the original channel list. Segmented and calibrated data is displayed in Fig. 2(b). The Channels pull-down menu shows the added process channels (marked on the menu). Data displayed in the image panels are the 300 kHz (top) axial and (bottom) circumferential channel.



(a)



(b)

Figure 3. Calibration curves generated simultaneously for all rotating probe channels from the GUI. Shown here are the phase-based depth curves for (a) +Point™ and (b) mid-range pancake coil at 400 kHz, 300 kHz, 200 kHz, and 100 kHz frequencies. The input values used for generating the curve are marked on each plot.

IV.3 Data Analysis Tools

A number of processes have been integrated into the user interface for off-line analysis of EC inspection data. Raw data acquired with certain EC test equipment can be uploaded directly and examined by using the available tools under the GUI. The processes are assembled under separate menus based on their function. Figure 4 displays the GUI panel along with the expanded view of four pull-down menus. The *ECTGUI* menu includes the functions associated primarily with loading, saving, and displaying of the data as well as a number of built-in MATLAB® functions, which were modified and adapted for use with the GUI. The *Measure* menu includes the list of routines that perform measurements along any arbitrary cross section or over a segment of data. Standard functions for the measurement of signal amplitude and phase are placed under that menu. The *Filters* menu includes a number of data manipulation algorithms that perform different operations on the data. Included in that list are the signal processing, detection, identification, and flaw sizing routines. Other useful tools such as those for simulation of noise and superposition of signals are also included in that menu. The *Scripts* menu includes functions that allow the user to create and modify MATLAB® script files that can be employed for automatic analysis of data. As noted earlier, the scripting tool permits sequential application of a series of user-defined processes to the data, thus providing the means for more efficient application of repetitive operations on a large number of files.

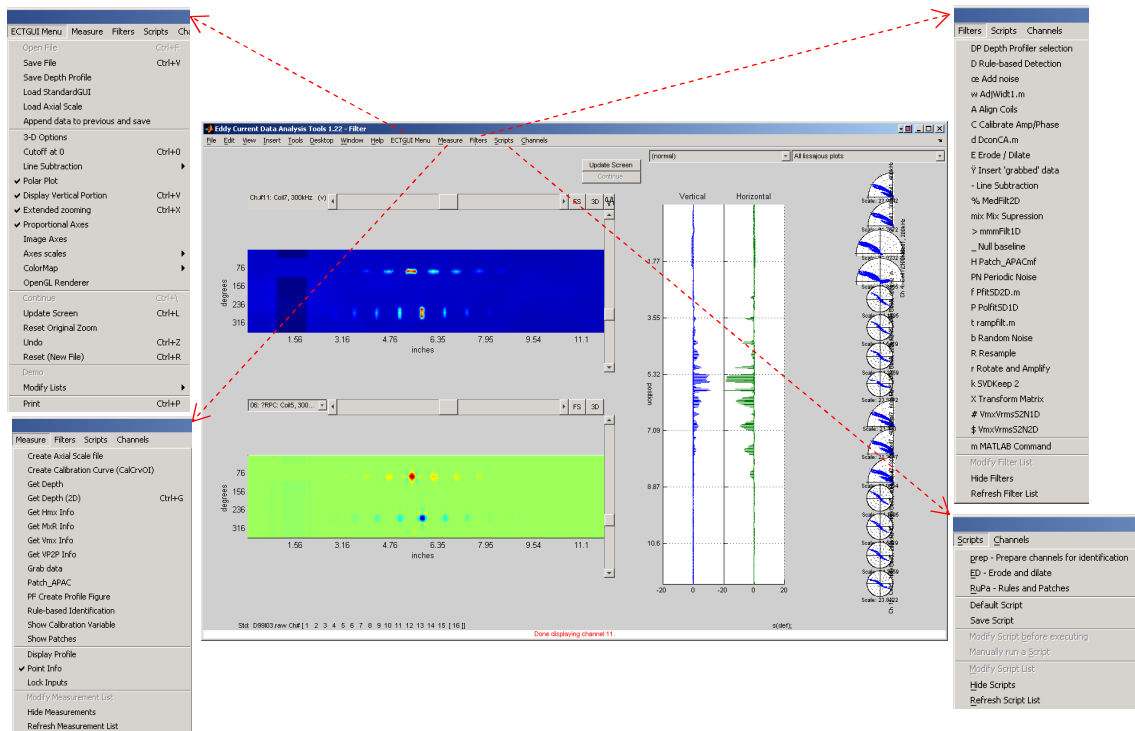


Figure 4. Data analysis tools available under different menus of the GUI. Shown here are the expanded views of current list of functions under four pull-down menus.

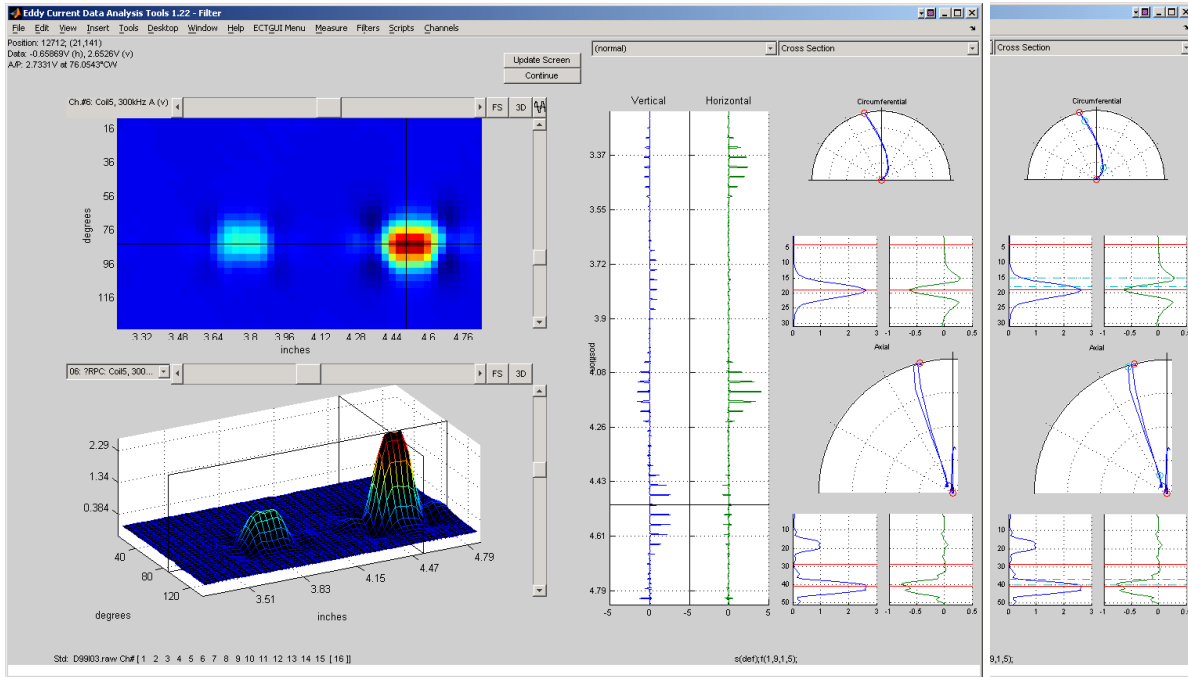
IV.3.1 Measurement Routines

In addition to the new routines, previous measurement routines have also been updated and made compatible with the new plugin system. They include algorithms for standard measurement of EC signals and for creating and applying of multiple calibration curves for estimation of flaw depth. Standard measurement algorithms duplicate the methods used by commercial data analysis software for measuring the amplitude and phase of the EC signals. Once the data is loaded, the graphical tools from the GUI may be used to make measurements of the amplitude and phase of a signal at any arbitrary position along the tube. This can be done either manually by scrolling through the data along the axial or circumferential direction, or automatically over a patch of data by using the function provided under the *Measure* menu.

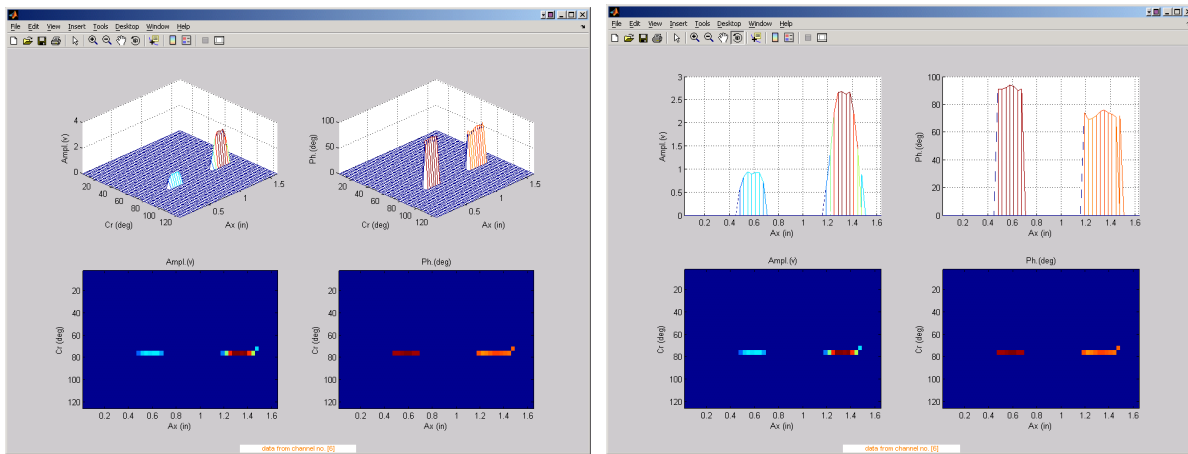
Because the GUI was intended to be used as an interactive research tool, the functionality is provided to manually analyze the data at any stage of the process. The functions provided under the *Measure* menu permit close examination of the data following each operation. This capability is particularly important for the evaluation of new user-developed algorithms. The measurements are performed simultaneously on all the available channels and the results are displayed in the command window. The option is provided to measure the signal either independently for each channel or relative to the primary channel by using the same positions for the maxima and the minima. Measurements may be made over discrete locations along the tube or successively along a line using the scroll buttons of the two-dimensional display panels. Flaw depth profiles may be generated by applying previously established calibration curves.

Alternatively, measurements could be made over a selected area of the tube in an automated manner. A peak detection algorithm that may be called from the measurement menu was developed for this purpose. The routine searches through the user-selected patch of data using a fixed-size kernel in order to locate and measure relevant signals. The default size of the measurement kernel is determined automatically based on the acquisition sampling rate and the tube diameter. Because the algorithm is threshold-based, it is best suited for application to small areas of the tube over which the peak signal amplitudes do not exhibit significant variations. The default threshold value may be changed by using the input dialog box in order to detect and measure weaker signals.

An example of signal measurements made from the GUI using the two methods described above is depicted in Fig. 5. The image display shows a segment of data from a calibration standard tube containing two axial OD notches. The EC inspection data was collected with a three-coil rotating probe. The analysis results here are based on the +Point™ probe response from the 300 kHz test frequency. Measurement of the signal corresponding to a single hit along the flaw length is shown in Fig. 5(a). The Lissajous displays on the left and right hand panes respectively show the peak-to-peak and the maximum rate of change measurements along the selected cross section for the signal amplitude and phase. Automated measurement over the entire data segment is displayed in Fig. 5(b). A separate display window shows the detected amplitude and phase values using the default value for the threshold. The estimated lengths of both indications are consistent with the 0.25-in. (6.35-mm) nominal length of the axial notches. The isometric and cross sectional plots of the same data are shown in different display panels. Built-in MATLAB® visualizations tools on these panels can be used to view the data from any arbitrary angle.



(a)



(b)

Figure 5. Representative graphics associated with the use of functions under the measurement menu. Shown here are (a) manual measurement of signal amplitude and phase based on peak-to-peak and maximum rate of change and (b) automated measurement of flaw signals over the same data segment from a calibration standard tube. The data segment displayed in the GUI includes a 60% TW and an 80% TW axial EDM notch detected with a +Point™ probe at 300 kHz.

IV.3.2 Filter Routines

Various signal processing and data analysis algorithms, generally referred to here as filters, have been assembled under a separate GUI menu bearing the same name. In addition to the incorporation of new filters, the routines developed earlier have been updated and made compatible with the new plugin system. The data analysis routines under the *Filters* menu currently include algorithms for pre-processing, detection, identification, and sizing of indications. The pre-processing routines consist of spatial and frequency domain filters intended primarily for suppression of noise or unwanted signals in general. Other routines assembled in the *Filters* directory include peak detection, rule-based identification, outlining of potential indications, and regression algorithms for sizing. The majority of the filters are applicable both to spatially one-dimensional and two-dimensional data. Certain routines, however, are applicable only to spatially two-dimensional data. Default filter parameters can be adjusted by using the dialog boxes at the beginning of the process. Further description of specific filter routines will be provided later in connection with the sizing algorithms.

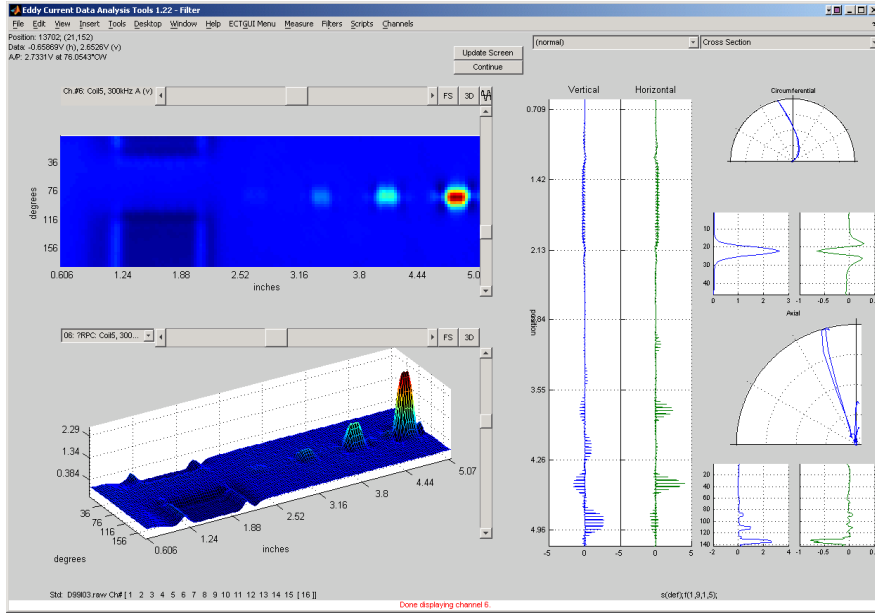
Although filter routines function in a similar manner as measurement routines, they differ in that unlike measurement operations filter operations modify the data. Furthermore, each time a filter is applied to the data the input parameters are stored and may be accessed by scripting routines at a later stage. The functionality is provided to reverse the operation of a filter routine. When filters are called, the process activates the *undo* function, which stores the data in its current state. The function may be used repeatedly to recover the original data. The undo function is particularly useful for testing of new algorithms and for the evaluation of data analysis methods.

Proper evaluation of EC inspection techniques and data analysis methods relies heavily on the availability of a suitable database. A viable approach to expanding of an NDE database with limited number of samples is to make use of the superposition principle. Algorithms developed earlier for superimposing of EC signals have been further refined and linked under the measurement and the filter menu. This tool can be used to simulate the response of an EC probe as a result of the influence of artifacts on nearby flaw signals or the interaction of closely spaced signals in general. Simulated data created in this manner may then be used to better evaluate the ability of signal processing and data analysis algorithms for detection and characterization of flaws.

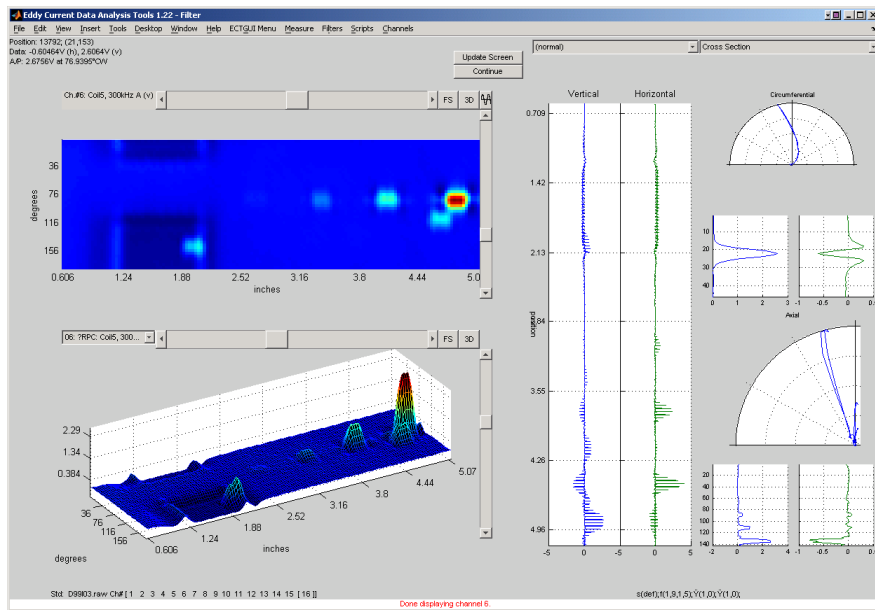
Improvements have been made to the superposition algorithms developed earlier to allow more transparent insertion of signals into a host tube. More flexibility is also provided with regard to the size of the selected data segment. The option is provided to apply the process to all or to specific set of channels. Different options are available for extrapolating of data at the edges of the inserted patch for optimally smooth transitions. Depending on the size of the data segment, the extrapolation and smoothing operations are performed on either two or all four edges of the data. Validation checks are also performed to ensure consistency of the channel configurations when superimposing data from different tubes.

Some examples are presented next to demonstrate the superposition of data by using the available tool under the GUI. Data collected with a rotating probe on an EDM notch standard tube is used first to demonstrate insertion of a signal into different locations on the same tube. Figure 6(a) displays the data from a section of the tube covering four OD axial EDM notches ranging from 20% TW to 80% TW and a portion of the simulated TSP collar. The functions under the *Measure* and *Filters* menu were used, respectively, to grab and insert a rectangular patch of data covering

the 60% TW flaw signal near the 80% TW flaw and at the edge of the TSP. The same tube section following the superposition operation is shown in Fig. 6(b). Although the graphics display the +Point™ probe response at 300 kHz, the process in this case was simultaneously applied to all the available channels. The isometric plots of the data do not exhibit any abrupt transitions in the periphery of inserted signals at either of the two locations where the signal was inserted. Another example of data superposition is presented in Fig. 7. In this case, data from a mock-up specimen covering an entire section of the tube that includes the TSP was superimposed on another (host) tube. Once again, the transitions at the two edges of the inserted data on the right hand side of the tube are reasonably smooth. Additional test cases on superposition of data are presented in connection with the evaluation of sizing results presented later in this report.

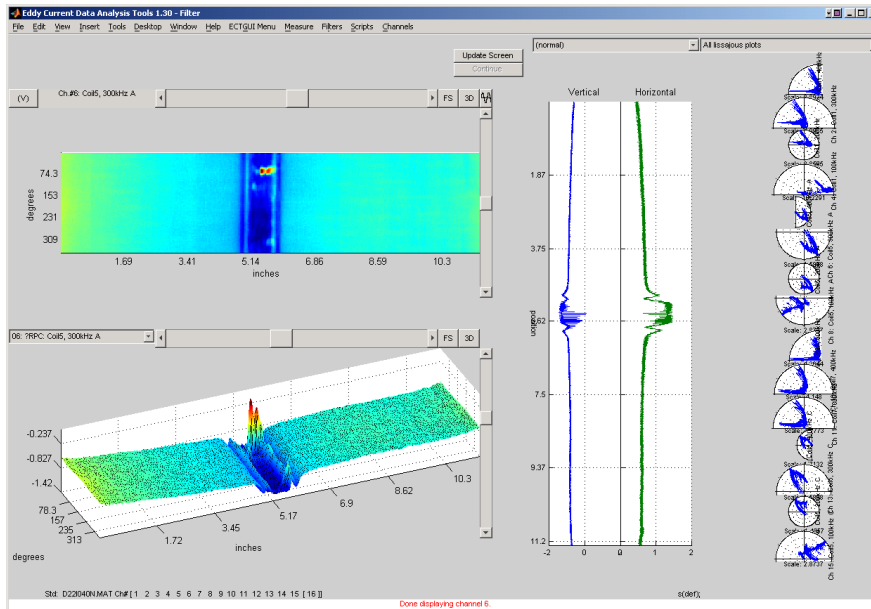


(a)

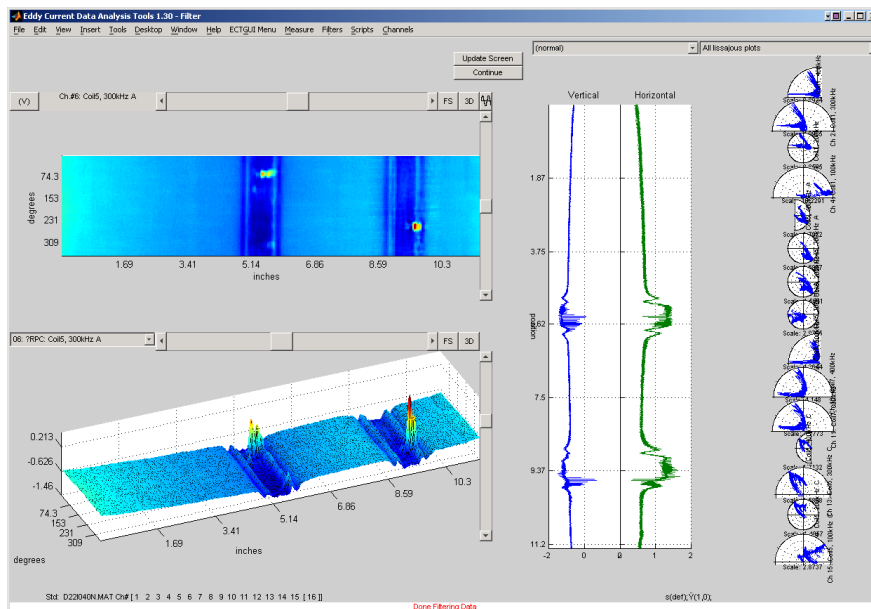


(b)

Figure 6. An example of data superposition tool used to simulate the effect of closely spaced signals and nearby artifacts on the probe response. The data segment used for demonstration is the portion of the calibration standard tube covering four OD axial EDM notches ranging from 20%TW to 80%TW and the simulated TSP collar. Displayed here are the +Point™ probe response at 300 kHz for (a) the original and (b) manipulated data with the 60% TW flaw signal inserted near the 80% TW flaw and at the edge of the TSP.



(a)



(b)

Figure 7. An example of data superposition tool used to insert rotating probe data from a 360° section of one tube into another tube. Graphics show (a) calibrated EC inspection data from a mock-up tube with multiple indications at a dented TSP region, and (b) the same tube with a second TSP section superimposed on it (near tube end on the right hand side). The superposition was simultaneously applied to all the test channels. Data displayed in the analysis window pertains to the +Point™ probe at 300 kHz frequency.

IV.3.3 Flaw Sizing Algorithms

The flaw sizing algorithms for rotating probes consist of a number of routines that perform various stages of the data analysis process. The common data manipulation stages consist of pre-processing, detection, identification, and sizing of indications. Post-processing of data prior to final estimation of the flaw size may also be selectively applied. This step is typically carried out to help restore any data points that might have been corrupted by the earlier stages of data manipulation. Pre- and post-processing of data is simultaneously applied to all the available channels. Flaw detection, identification, and sizing routines on the other hand operate only on the set of user-defined channels.

Pre-processing of data is initially performed to help suppress the influence of unwanted signals and background noise. Both spatial and frequency domain filters have been developed to help improve signal-to-noise ratio (S/N). Selection of an appropriate type of filter will depend on the nature of unwanted signals. In general, a deterministic rotating probe response from artifacts such as TSPs is more effectively suppressed by using spatial domain filters. The types of noise with specific frequency spectrum are often suppressed more effectively by using frequency domain filters. Other signal suppression techniques such as least-squares-based multi-frequency mix algorithms and spectral decomposition algorithms have also been incorporated into the data analysis tool and may be used on an application-specific basis. Reduction of random background noise, either associated with the instrument's electronics or with slight trigger-related misalignments, may also be achieved by smoothing of data. Polynomial fitting algorithms optimized for typical EC inspection data are currently used for this purpose. The routines automatically calculate as the default values the operating kernel size and the polynomial order based on the sample rate of the data. The option, however, is provided to adjust the default values as necessary. It is worth noting that any filtering process is expected to influence the signal amplitude and phase to a certain degree. The default values for the filter parameters are generally set such that they provide optimal tradeoff between improving of S/N and distortion of the probe response. Thus, a viable approach to evaluating the influence of filter parameters on signals in the tube data being analyzed is to first apply the identical processes to the calibration standard tube.

The detection routine employs a threshold-based algorithm that first partitions the data into a number of smaller regions. The data is initially subdivided along the lines of minimum variance that delineate the regions of interest (ROIs) for subsequent processing. The number of data segments generated in this manner may not always represent the minimum number of ROIs containing relevant signals. Various algorithms were examined for partitioning of the data into minimum number of ROIs with relevant indications. Reduction of the original number of ROIs was achieved by linking of the segments with baseline data to adjacent segments that contain signals above a threshold. The segmentation process for two of the algorithms evaluated in those studies is illustrated in Fig. 8. Figure 8(a) illustrates how data from a tube may be divided up into a large number of ROIs following the initial segmentation based on the lines of minimum variance. Five rectangular patches of data with potential indications are marked on the figure. Figures 8(b) and (c) illustrate two possible outcomes for linking of the two patches of data with no relevant signals, marked as A and B, to their neighboring ROIs. For the first approach, no assumption was made regarding the correlation of a data point with its nearest neighbors. For the second approach, the assumption was that helically scanned data collected with a rotating probe are more correlated along the circumferential direction. Tests performed so far indicate that, while the segmentation based on the first approach, shown in Fig. 8(b), often results in a more uniform distribution of ROIs, it also has the potential to create gaps among those regions. The results based on the

second algorithm are illustrated in Fig. 8(c). The process in this case is more computationally efficient and has proven to be more robust in linking of ROIs.

The detection process employs a search routine that locates and measures all the flaw-like signals along the orthogonal directions over each ROI. The operation can be performed over the entire EC inspection data from a tube or over a user-defined segment. The peak detection routine provides the option to select the type of measurement for the signal amplitude and phase. The default measurement type is set to the peak-to-peak value. The threshold-based detection algorithm also takes into account the signal shape in order to separate the potential flaw signals from artifacts. Both absolute and relative (to the peak signal amplitude) thresholds are used for the detection of signals within each ROI.

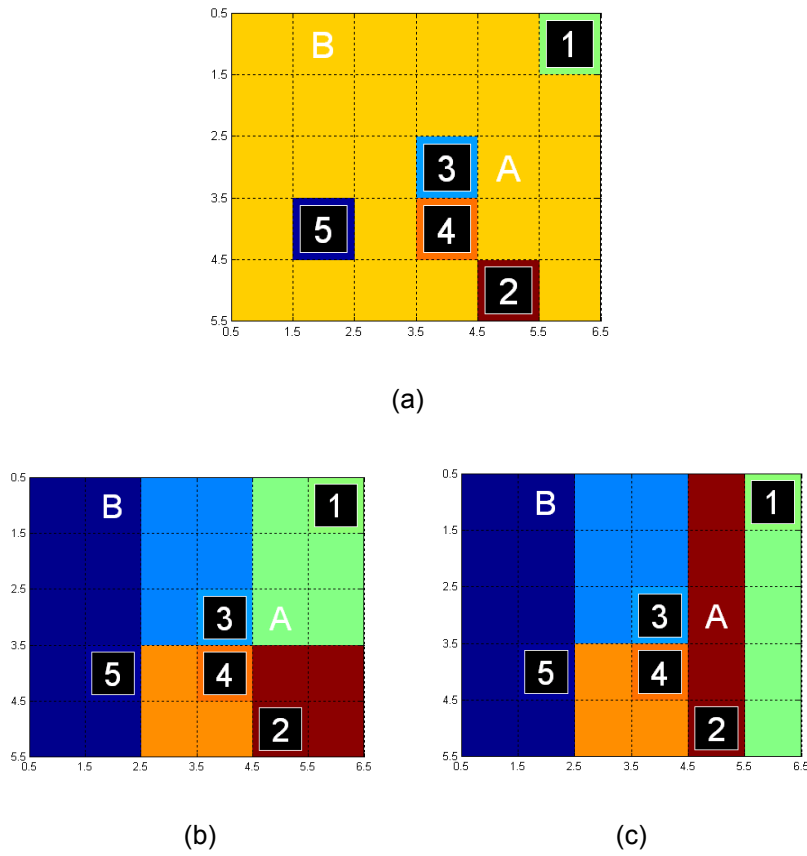


Figure 8. Illustration of the segmentation process for two algorithms evaluated to determine the optimal approach for processing of EC inspection data over the entire length of tube. Threshold-based initial segmentation of data with five ROIs is illustrated in Fig. 8(a). The following drawings in Figs. 8(b) and (c) illustrate two possible outcomes for linking of the small patches of data with no relevant signals, marked as A and B, to their neighboring ROIs. While the segmentation shown in Fig. 8(b) often results in a more uniform distribution of ROIs, it can lead to their improper linkage resulting in potential gaps. The result based on the second algorithm that assumes helically scanned data is more correlated along the circumferential direction is illustrated in Fig. 8(c). The process in this case is more computationally efficient and has proven to be more robust in linking of ROIs.

Identification of relevant flaw signals from tubing artifacts is done by employing a rule-based algorithm. A set of predetermined conditions are used to decide whether a signal should be kept or eliminated based on its origin and its general characteristics. The bounding values are determined based on the amplitude and phase relationships among different test frequencies for known signals from a calibration standard tube. In addition to the general rules, empirical rules are also included in that set. Although the coefficients that set the bounds for acceptable range of signal variation may be adjusted for specific test conditions, the default values are generic and are intended to apply to a wide range of test conditions. Information from a minimum of two channels, typically consisting of a primary and an auxiliary test frequency, is needed for this stage of the process. The use of a larger number of test frequencies, however, is expected to improve the ability to identify the flaw signals.

As noted earlier, post processing operations are selectively applied to recover the data points that might have been corrupted by the previous operations. A subset of filters used for pre-processing of data is typically used for post-processing operations. Polynomial interpolation is typically used for this purpose. The interpolation may be carried out in number of directions including axial, circumferential, diagonal, or in a semi-circular pattern. Morphological operations may also be employed for post processing of data. The erosion and dilation algorithms have been included in a single routine under the *Filters* menu. The erosion operation is intended for removal of sharp and isolated data points. The dilation operation on the other hand attempts to fill in the missing data points based on its relationship to its nearest neighbors. Although default kernel sizes are provided for morphological operations, these values may be adjusted through input dialog box for the filter.

The final estimate of the flaw size in a tube can be generated by using the data from either a single channel or from multiple channels. Different options are currently available for calculating the flaw depth based on the signal amplitude, phase, or both pieces of information. A multiple linear regression algorithm is employed for calculation of depth from multiple test frequency data. A set of dynamic functions have been implemented which convert the processed data into final estimate of flaw depth. These algorithms currently allow calculation of the flaw depth based on the available data from a single test frequency or from multiple test frequencies. Alternate methods using the amplitude, phase, or the combined amplitude and phase (hybrid) information can currently be applied to estimate the flaw depth. The option is also provided to estimate the depth of an indication based on the minimum, maximum, mean, or the median of all the values predicted by the different test frequencies. For multi-frequency inspections, this option allows for different degrees of conservatism when estimating the depth an indication. This approach may be particularly useful for sizing of low-amplitude indications for which significant variation could exist among the predicted depths at different test frequencies or by different coils.

A new function under the *Filters* menu named *Depth Profiler* allows the user to select from the list of available options the method for estimating the depth of indications in a tube. This function in turn creates a new plugin system for generating the depth values. When first activated, a dialog box containing a list of the existing routines in the *Profilers* directory allows the user to select the desired depth sizing method. Profilers are dynamic processes that map the phase and amplitude information into estimates of flaw depth. The sizing data for ID and OD originated indications are displayed in separate panels of the analysis window. Activation of the viewer under the *Measure* menu allows the depth values to be displayed over the entire tube. The GUI stores the sizing data rather than recalculating the depth values every time the function is called. This makes the process more efficient and adds flexibility to the types of depth profiles that can be generated. Once the *Profiler* is activated, the sizing data is automatically updated each time the processed data

is modified. The updating of sizing data occurs following the application of a new filter or script and following modification of the channel list. The sizing results are stored in a global variable, which allows the data to be reloaded and viewed by the GUI or by another MATLAB® routine at a later time.

Several examples on sizing of indications based on rotating probe data acquired from the ANL/NRC tube bundle mock-up sections are provided later in this report. The examples describe various stages of the data analysis process for generating the final estimate of flaw size either over a selected section of the tube or over the entire tube. Representative cases on final estimation of flaw size based a single or multiple test frequency is presented. In addition to the conventional phased-based depth sizing, the results of comparative studies are also presented on the employment of alternative sizing methods employing both the amplitude and phase information.

IV.3.4 Scripting Tool

As noted earlier, functions are provided under the *Scripts* menu of the GUI for automatic creation of MATLAB® scripts. Scripts allow multiple user-defined processes from the *Filters* menu to be applied sequentially to the data. The scripting tool is particularly useful for efficient processing of a number of data files that are to be manipulated in a similar manner. New data files may be analyzed quickly once the processing steps have been determined. Major refinements have been made to the scripting tool under the new plugin system. The new software structure supports multiple character 'keys' and permits an arbitrary number of filters to be included in the scripts file. A script can be saved at any time during the data analysis process using the embedded function from the *Scripts* menu. The script is saved as a standard MATLAB® text file (m-file) and may be later modified manually if necessary.

A sample script that was generated automatically using the scripting tool from the GUI is shown in Fig. 9. Figure 9(a) displays the set of processes (filter 'keys' are marked on the bottom right corner of the analysis window) which were applied to the rotating probe data from a mock-up tube section. The text of a script file containing all the processes and their associated arguments are shown in Fig. 9(b). The file contains a list of common steps used for analyzing of rotating probe data. Each processing step is identified by a filter number. The call to that particular filter and its associated arguments are included in a single line. The filters listed in the sample script include the pre-processing, rule-based identification, signal detection, and depth sizing routines. While the script file made available for viewing and modification is relatively simple, for certain functions, the actual script that performs the operations on the data may have more detail that is hidden from the user. The arguments for certain processes in the script file may be modified at any time. Updating of the script list from the analysis GUI will automatically load any new script file under the *Scripts* menu.

The format of a typical script includes information about the script's name, its unique identifier (UID), menu *key*, and visual shorthand of its content. Also included in the structure of individual filters is the name, menu 'key', UID, version, and the associated array of the input parameters. Under the new plugin system, a more extensive file validation and error checking has also been incorporated into the scripting tool. Error checking is done to ensure that the version of the filter routine being applied to the current data is consistent with that used when the script was first generated. A new script may easily be linked into the GUI by placing the file in the *Scripts* folder and refreshing of the menu.

IV.3.5 Incorporation of User-developed Algorithms

As noted earlier, the primary motivation behind implementation of the new plugin structure of the data analysis GUI was to allow inclusion of new and updating of existing data processing routines independent of the core program. User-developed scripts under the new configuration may be edited and tested without affecting the functionality of the main GUI. A brief description of modifications and refinement of measurement and filtering algorithms is provided below.

Modification of measurement and filtering routines under the previous version of the user interface for the analysis of EC inspection data typically required manual editing of a complex structure. That approach, which involved storing of variables in long strings, complicated the scripting of user-developed functions. Furthermore, improper storing of a particular variable could potentially affect the functionality of the main GUI itself. Although attempts were made along the way to alleviate those problems, a new structure had to be devised in order to eliminate those shortcomings altogether. With the new structure, each measurement or filter function is a separate plugin file that is independent from the rest of the structure. This approach limits the possibility of errors propagating through the rest of the structure. Also, because the functions are now regular MATLAB® text files, they are easier to interpret and edit.

A simple example for creating and executing a filter routine under the new plugin structure is presented here. It should, however, be noted that a typical filter intended for modifying of the data contains additional information such as UID and input parameter associated with that filter. The top pane in Fig. 10 displays the text of a filter routine that was generated for demonstration purposes only. The comment lines at the top define how the plugin is loaded into the GUI. In this case, the function name is “Subtract mean of the data” with an identifier ‘key’, “mn”. Subsequent comment line section defines what happens when this plugin is called by the main GUI. In this case, the MATLAB® filename (*%mfilename%*) would be replaced by the current name of the file. Additional comments may arbitrarily be added to this section as needed. The bottom section of the file contains a simple code that subtracts the mean value from the data. Once the filter menu is refreshed, the code is automatically loaded under the filter list. The outcome of this stage is displayed in the middle pane of Fig. 10, where the new filter name with the associated ‘key’ is highlighted as the first function under the *Filters* menu. Finally, the bottom pane in Fig. 10 displays the results following execution of the filter routine that was called from the main GUI. Also shown is the calculated mean value in the command window. The multi-character filter key that was added to the sequence of scripts is also marked on this figure.

```

1 % PluginName='Subtract mean of the data';
2 % PluginKey='mn';
3 %
4 % :CALLBACK:
5 % %mfilename%;
6 % :CALLBACK:
7
8 meandat=mean(mean(FiltData));
9 disp(['mfilename ' : The mean value of FiltData is: ' num2str(meandat) ]);
10 FiltData=FiltData-meandat;
11

```

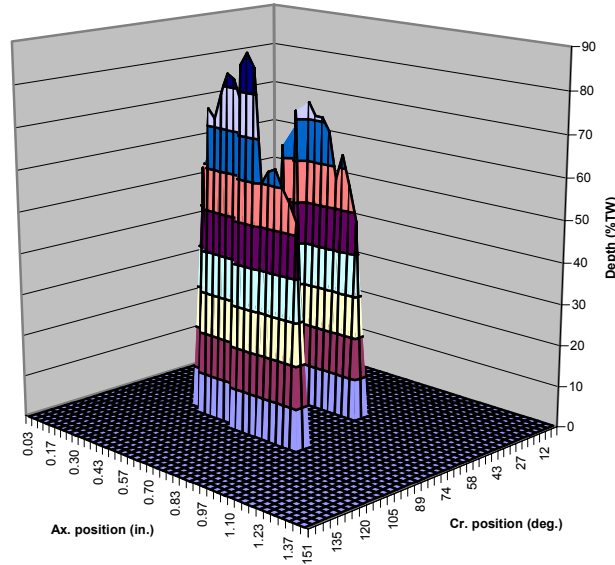
The screenshot shows the software's GUI. On the left, the 'Filters' menu is open, with 'mn Subtract mean of the data' highlighted at the top. A red circle highlights this menu item, with a callout box stating 'New filter name added to menu'. The main window displays several plots: 'Vertical' and 'Horizontal' waveforms, and 'Circumferential' and 'Axial' cross-sections. A red circle highlights the 'mn' key in the bottom right of the plot area, with a callout box stating 'Multi-character filter 'key' added to script list'. At the bottom, the command window shows the output: 'Filters_0000_Example: The mean value of FiltData is: -0.034244+0.034897i' followed by '>>'. A red circle highlights the 'mn' key in the command window output, with a callout box stating 'Command window display of filter application and final results'.

Figure 10. A simple example for creating and executing a filter routine under the new GUI plugin system. Displayed here are (top) text of a file for a simple filter routine that was generated for demonstration purposes, (middle) inclusion of the new filter name as the first item under the *Filters* menu following refreshing of the list and display of the multi-character filter 'key' at the bottom the analysis window following its application, and (bottom) result of the operation on data displayed in the command window.

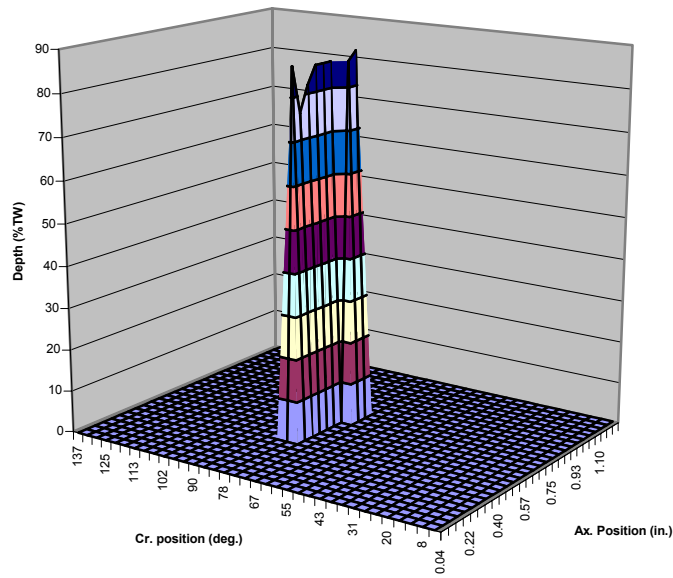
IV.3.6 Exporting of Data

Under the new plugin structure of the GUI, additional functionality has been incorporated for exporting of data. Currently, multi-frequency EC inspection data loaded into the GUI can be saved directly into a standard MATLAB® data file (binary format) at any stage of the data analysis process. Data over any arbitrary section of the tube may be saved in this manner. Data may also be exported to a text file following the initial calibration stage. In this case, two separate files containing the horizontal and the vertical components of the data from the current channel that are visible in the display panel will be saved. Additional options to export the final sizing data to a text or an Excel™ file are also provided. In that case, the sizing results from the selected section of a tube are saved along with the axial and circumferential positional information. More robust error checking has also been added to ensure that all data types are saved in the appropriate format.

The efforts on the development of routines for exporting of data outside the MATLAB® environment were prompted in part by the need to use the NDE results for other studies. Under a separate task, the NDE sizing results were used as input to mechanistic models for the prediction of tube failure pressure and leak rate. An example of sizing results that was converted to a standard format for independent manipulations is shown in Fig. 11. Data analysis results were exported and subsequently read by using the Microsoft Excel™ software. The results here pertain to the sizing of laboratory-produced cracks in two mock-up tube specimens. The flaws were identified as OD-originated single and multiple axial indications. Data was exported for a small region of the tube containing the flaws. The isometric plots display the estimated depth values as a function of axial and circumferential position.



(a)



(b)

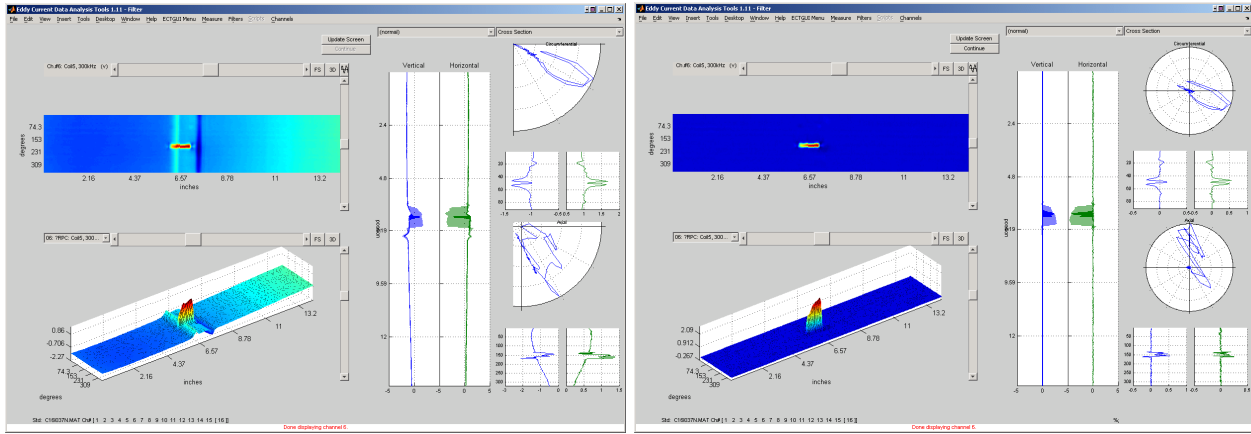
Figure 11. Representative Excel™ plots generated from the output of data analysis GUI. A script has been implemented that allows exporting of the final sizing results into text format. Results shown here are exported sizing results for indications in two mock-up test sections with (a) multiple and (b) single OD axial crack that are part of the data set selected for studies associated with the equivalent rectangular crack model.

V. Test Case Results on Flaw Sizing

Representative test cases are presented next on sizing of SG tubing flaws based on rotating probe data. The examples demonstrate how the tools currently embedded in the data analysis GUI may be used to analyze EC inspection data. The rotating probe data used in these investigations were collected earlier from a subset of mock-up tube sections with laboratory-grown cracks. The majority of the tubes included in the data set contained deep flaws. Selection of the specimens was based in part on the criteria set under parallel studies on the evaluation of tube structural integrity. As noted earlier, the NDE estimate of the flaw size in a subset of specimens was used as input to mechanistic models for the prediction of tube failure pressure and leak rate. The results those investigations will be published in a separate report.

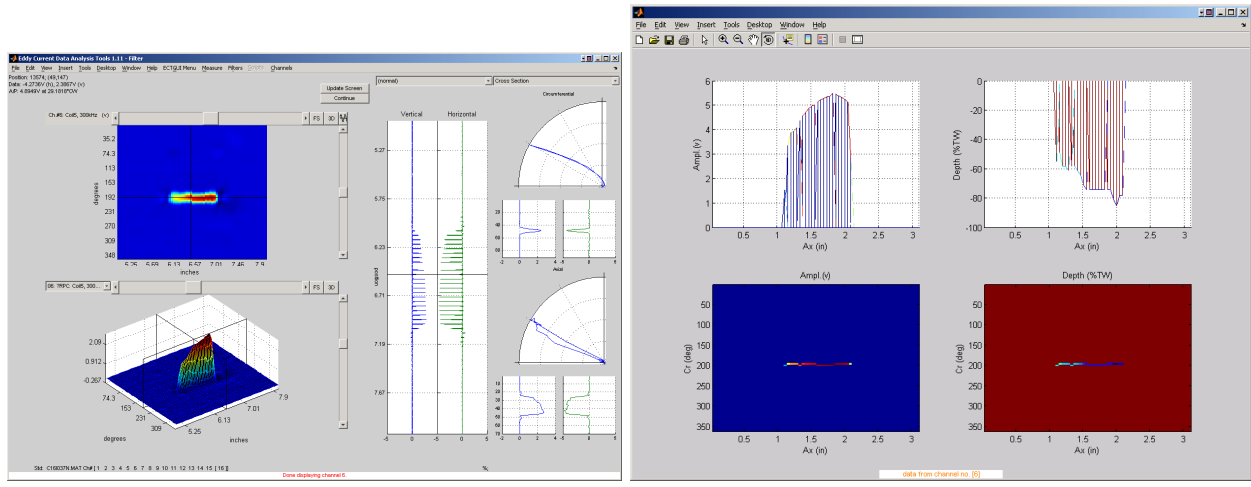
Eddy current rotating probe data was used to estimate the size of flaws in a number of mock-up tube specimens. Data on all the tube sections was collected with a three-coil rotating probe, which employs a mid-range 0.115-in. (~3-mm) -diameter pancake coil, a +Point™ coil, and a high-frequency 0.080-in. (~2-mm) -diameter pancake coil, with all the coils embedded in a single probe head assembly. The analysis results presented here pertain only to the +Point™ data. The database of tubes used in these investigations included both axial and circumferential SCCs, with the majority of the flaws being OD initiated. The specimens contained either single or multiple indications located in one particular region of the tube (i.e., either free-span or TSP). In order to better evaluate the ability of the algorithms to detect and size flaws over the entire length of a tube, the original data set was augmented with simulated data. The data superposition tool under the GUI was used to compensate for the lack of specimens with discrete indications located at different regions of the tube.

Data analysis results are presented first on sizing of cracks over a selected region of a tube. The sizing results are provided for two tube specimens containing an ID and an OD originated flaw, respectively. Figure 12 shows different stages of the data analysis process for sizing an indication located in the TSP region of the of the first. Figure 12(a) shows the main analysis window with the calibrated data from the +Point™ coil at 300 kHz being displayed in various formats. The entire length of the tube is displayed in image, isometric, and strip-chart plots. Axial and circumferential cross sections of data for an arbitrarily selected location are plotted on the Lissajous figures. Filtered data after suppression of the TSP signal is shown in Fig. 12(b). A spatial domain median filter was employed in this case to remove the probe response associated with the axisymmetric TSP. Figure 12(c) shows the same data for a short section that includes the flawed region of the tube. Following the application of rule-based identification and signal detection routines, the final sizing results are shown in Fig. 12(d). Except for the detection and sizing, all other operations were performed on data over the entire length of the tube. The amplitude and depth profiles for the segment of the tube including the flaw are displayed in cross sectional plot and in image format. The separate panel for displaying of the final sizing results was created by using the display tool available under the measurement menu. To distinguish between OD- and ID-initiated indications, the depth profile for the former is plotted as positive values and for the latter as negative values, both as a function of position. The results in this case indicate presence of a ~1-in.-long ID crack with a maximum depth of slightly larger than 80% TW. The results on sizing of a free-span ODSCC in another test section are shown in Fig. 13. Data analysis stages shown here correspond to those displayed Fig. 12. Also, the processes used for the analysis of data in this case were identical to those used in the previous test case. The sizing results shown in Fig. 13 (d) suggest presence of a >1-in. long axial crack with a maximum depth of >90%TW.



(a)

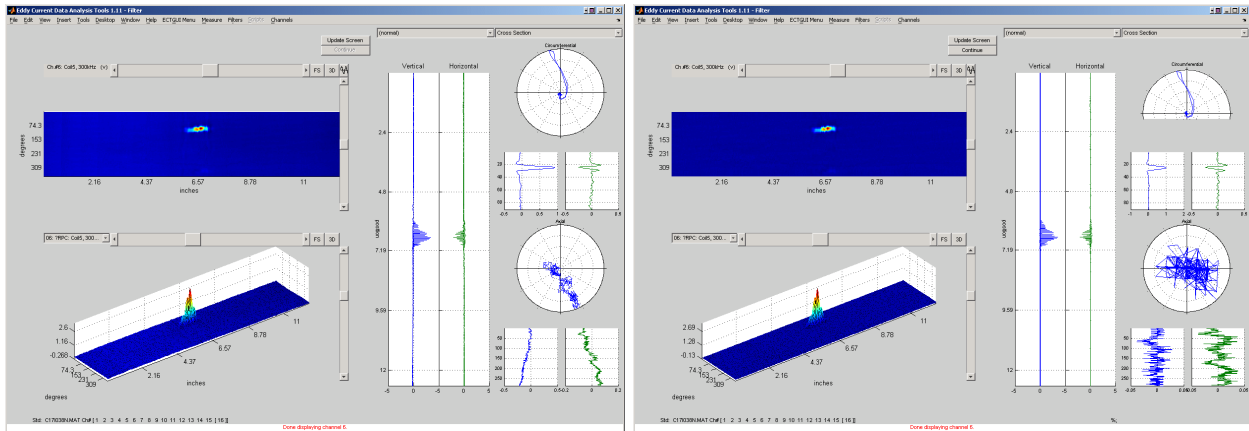
(b)



(c)

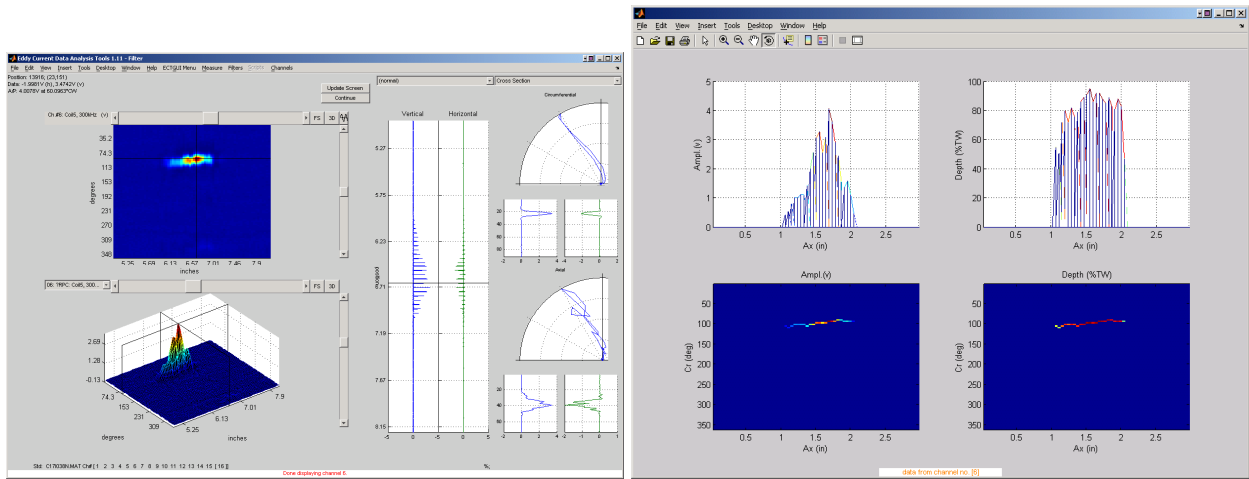
(d)

Figure 12. Display of data at various stages of the process for sizing of and an ID initiated indication in a mock-up TSP test section. Graphics show (a) the +Point™ data for the entire tube section at 300 kHz in various display formats, (b) filtered data after suppression of the TSP signal, (c) filtered data over a short section covering the flawed region of the tube, (d) the sizing results displayed in a separate window and with amplitude and depth profiles displayed in cross sectional plot and in image format. The results in this case indicate presence of a ~1-in.-long ID crack with a maximum depth of slightly deeper than 80% TW.



(a)

(b)



(c)

(d)

Figure 13. Display of data at various stages of the process for sizing of and an OD initiated indication in a mock-up free-span test section. Graphics show (a) the +Point™ data for the entire tube section at 300 kHz in various display formats, (b) filtered data after suppression of the TSP signal, (c) filtered data over a short section covering the flawed region of the tube, (d) the sizing results displayed in a separate window and with amplitude and depth profiles displayed in cross sectional plot and in image format. The results in this case indicate presence of a >1-in.-long OD crack with a maximum depth of >90% TW.

Data analysis results are presented next for three other test sections containing single and multiple cracks. The tube sections were identified as having OD-initiated SCCs with either axial or circumferential orientation. Once again, the flaw sizing was done over a user-defined region of the tube and employing the same analysis procedure as before. Figure 14 displays the rotating probe data at different stages of the process for sizing of a flaw in a test section containing multiple axial indications. Figure 14(a) shows the analysis window with the calibrated +Point™ data displayed in various graphical formats. The signals from the axial indications in the tube extend outside the TSP edge. Filtered data following the suppression of the TSP signal is shown in Fig. 14(b). The data in that figure shows a short segment of the tube containing the flawed region. The final sizing results following the detection, identification, and post processing of data are shown in Figs. 14(c) and (d). The two panels display the same data from different view angles. Once again, the amplitude and depth profiles are shown in cross sectional plot and in image format. The images show two nearly parallel axial cracks of different lengths that are less than 50 degrees apart circumferentially. Axial profile of the longer (~0.5 in.) crack displayed in Fig. 14(c) shows a maximum depth of >90% TW. Circumferential profile for the same data, which is shown in Fig. 14(d), suggests the maximum depth of the shorter crack (~0.25 in.) to be >80% TW.

The results on sizing of another test section containing a short axial flaw is shown in Fig. 15. The indication in this case is confined within the TSP region. The results shown at different stages of the process here correspond to those displayed in Fig. 14. The sizing results displayed in Fig. 15(c) suggest presence of a short (~0.2-in. long) axial crack with a maximum depth of ~90% TW. The sizing result for another tube specimen with circumferential cracking is shown in Fig. 16. Some intermediate stages of data analysis are shown in Figs. 16(a) and (b). The final sizing results are shown in Fig. 16(c). The results in this case indicate presence of circumferential cracking that extends >200° around the tube with an average depth of <60%TW and a maximum depth of ~70% TW. It is worth noting that comparison of the data in the above examples indicate that SCC signals with significantly different amplitudes can have comparable depth estimates.

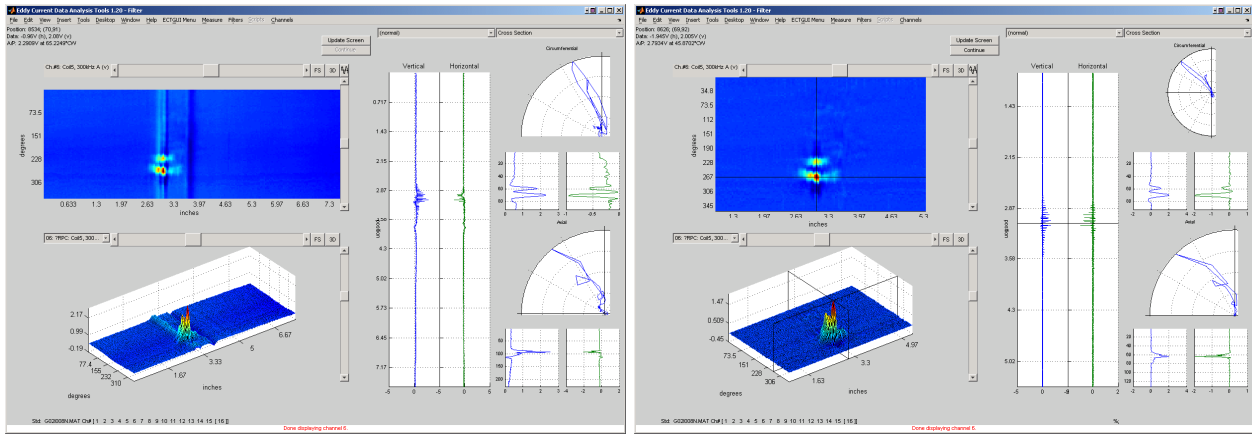
As noted earlier, alternative methods have also been investigated as part of the studies on sizing of SG tubing flaws based on rotating probe data. One of the viable approaches examined to date is to incorporate the amplitude information to complement the phase-based estimates of the flaw size. With this method, the amplitude-based sizing is applied to those parts of the flaw signal that may otherwise be eliminated because their amplitude lies below the threshold set for phase-based sizing. In effect, the amplitude is used when the phase angle of the signal cannot be reliably measured (e.g., often near the flaw ends). Representative test cases are provided next on sizing of indications by using the combined information from the measured amplitude and phase (hybrid sizing) of a signal.

The analysis results for three flawed tube specimens are presented in Figs. 17 to 19. The indications were located either at the TSP or at the free-span region of the tube, all in conjunction with tube denting. The hybrid sizing algorithm was used to generate the final estimates of the flaw depth. Figure 17 shows representative graphics from various stages of the data analysis process for a tube section with multiple axial indications at a dented TSP region. The calibrated +Point™ data for the entire tube section at a test frequency of 300 kHz is displayed in Fig. 17(a). The processed data over a short section covering the flawed region of the tube following the pre-processing and rule-based identification stage is shown in Fig. 17(b). The final estimate of the flaw size following the detection and post processing stage is displayed in Fig. 17(c) in a separate panel with the amplitude and depth profiles displayed in cross sectional plot and in image format. The results in this case indicate presence of two OD initiated axial SCC with the longer flaw having a length of slightly greater than 1-in. with an average depth of ~60%TW and a maximum depth of

<70% TW. The depth estimates, all below 10%TW, for the small sections at both ends of the flaw were made by using the amplitude information. Comparison of the sizing results here with depth estimates made based only on the phase angle data (not shown here) demonstrated that the hybrid algorithm produces a more conservative estimate of the flaw length.

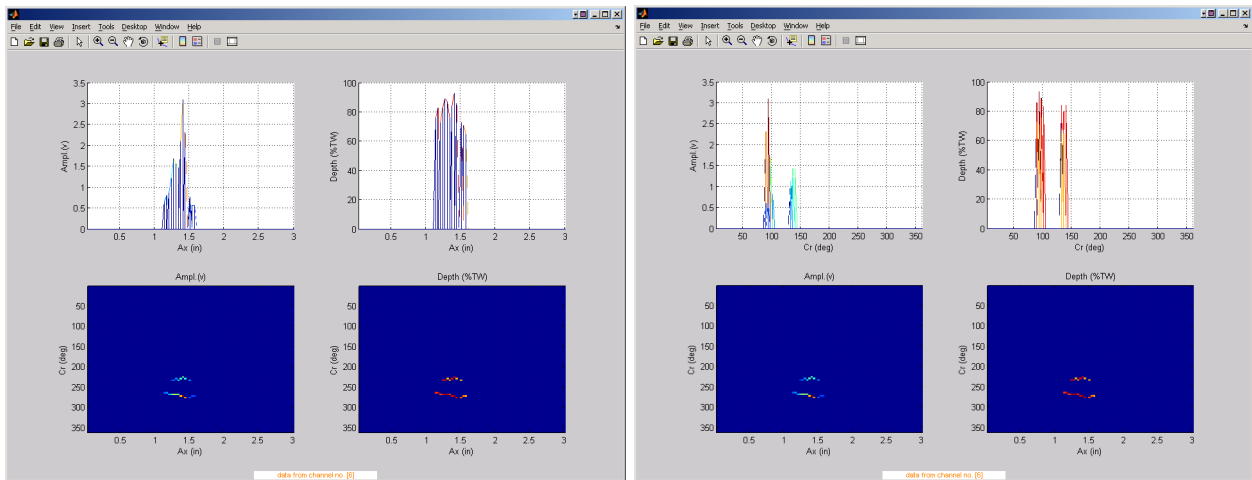
Data for another tube specimen with multiple signals at the TSP region is shown in Fig. 18. The data analysis stages for this case correspond to those shown in Fig. 17. The final sizing results displayed in Fig. 18(c) indicate presence of two axial SCC of OD origin with the longer flaw having a length of <1-in. and a maximum depth of ~70% TW. Once again, the threshold-based hybrid sizing results once again produced a slightly more conservative estimate of the flaw length in comparison with the sizing based on the phase angle alone. Figure 19 displays the analysis results for a low amplitude indication (<0.3v peak-to-peak) in the free-span region of the tube. In addition to denting, the EC data in this case had relatively high level of baseline noise as shown in Fig. 19(a). Filtered data over a small region of the tube containing the flaws is shown in Fig. 19(b). The pre-processing of data resulted in nearly complete elimination of the baseline noise. The final sizing results shown in Fig. 19(c) indicate presence of multiple OD axial indications with the largest indication having a length of >0.25-in. and a maximum depth of <70% TW.

The eddy current inspection data from the three tube sections shown in Figs 17-19 also served to further evaluate the rule-based algorithm that is used as an intermediate stage of the data analysis process. These samples were chosen because they all contained tube denting. The influence of tube deformation such as dents on a nearby flaw signal could pose a particular challenge to such algorithms. The flaw sizes in the three tube sections shown in Figs. 17-19 were first estimated without applying the rules. The sizing result in all cases suggested significant underestimation of the depth for those parts of the flaw signal which were located near the peak response from the dent. The flaw sizes were subsequently estimated after the application of rules. As demonstrated by the three examples here, in all test cases the application of the rules resulted in reasonable suppression of the probe response from dent and in turn a more conservative estimate of the flaw size.



(a)

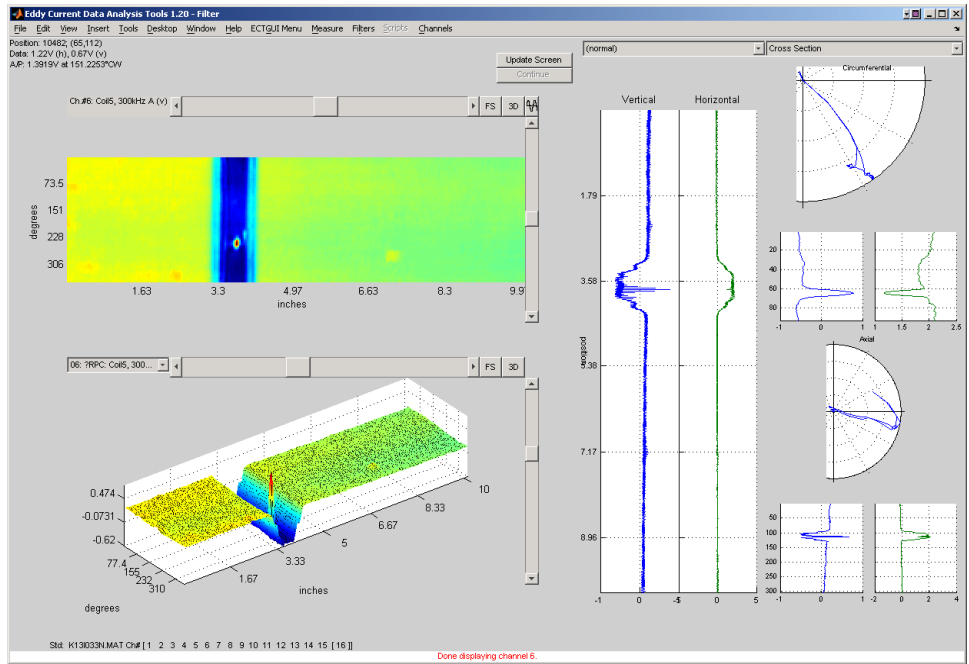
(b)



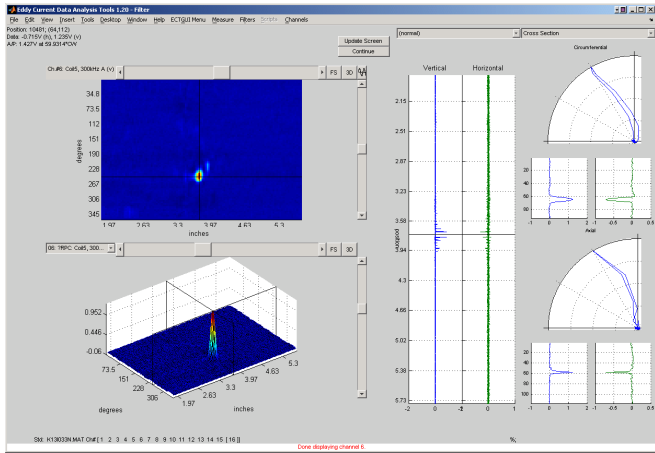
(c)

(d)

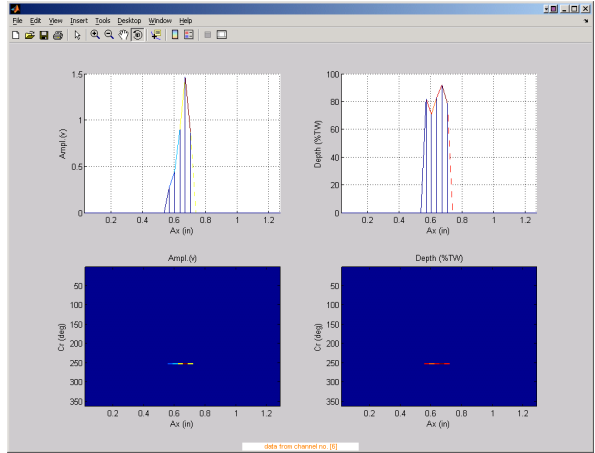
Figure 14. Display of data at various stages of the process for sizing of OD initiated multiple axial indications in a mock-up tube section. Graphics show (a) the +Point™ data for the entire tube section at 300 kHz in various display formats, (b) filtered data over a short section covering the flawed region of the tube, and (c) axial and (d) circumferential profile of the flawed region. The sizing results are displayed in a separate window with amplitude and depth profiles displayed in cross sectional plot and in image format. The results in this case indicate presence of two nearly parallel axial cracks of different lengths that are $<50^\circ$ apart circumferentially. Axial profile of the longer (~0.5 in.) crack displayed in Fig. 14(c) shows a maximum depth of $>90\%$ TW. The circumferential profile shown in Fig. 14(d) suggests the maximum depth of the shorter crack (~0.25 in.) to be $>80\%$ TW.



(a)

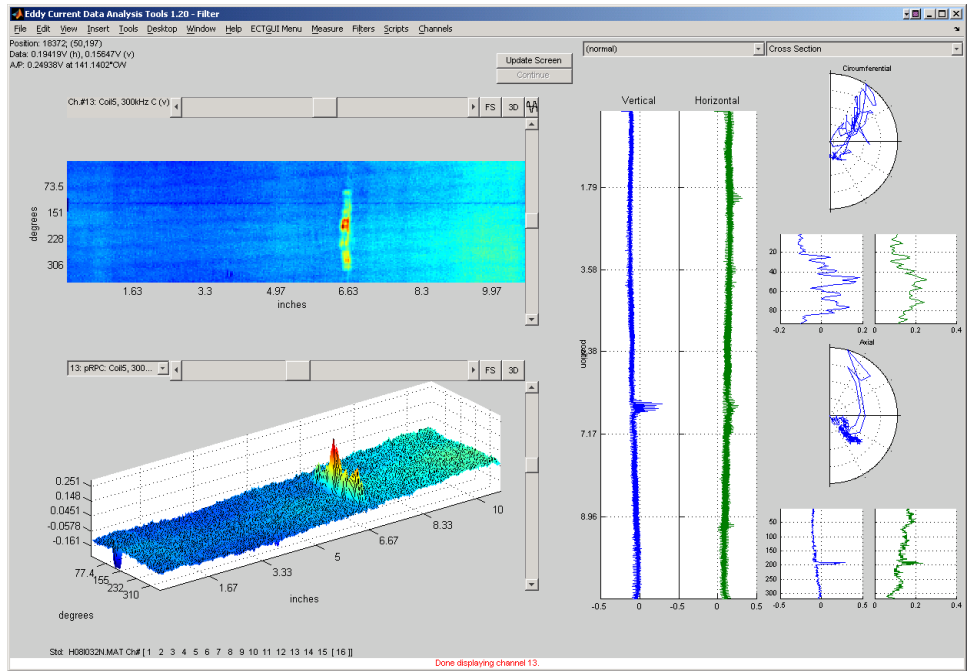


(b)

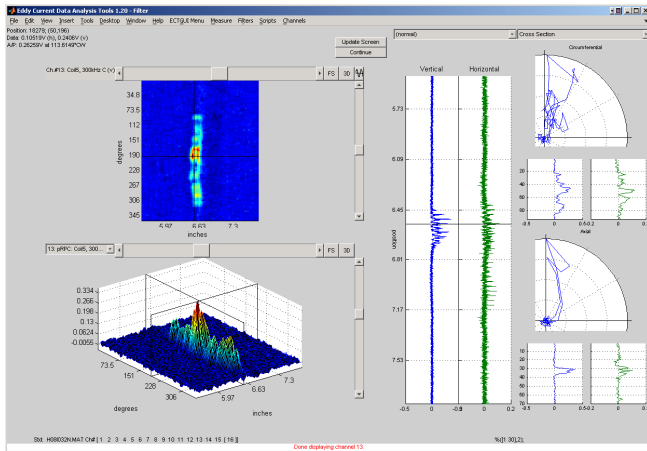


(c)

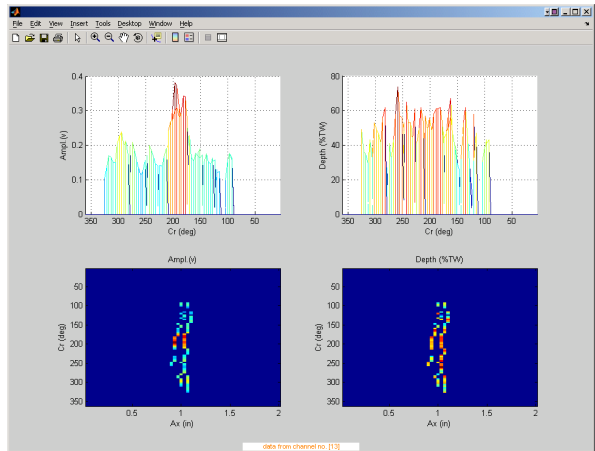
Figure 15. Display of data at various stages of the process for sizing of OD initiated axial indication in a mock-up tube section. Graphics show (a) the +Point™ data for the entire tube section at 300 kHz in various display formats, (b) filtered data after suppression of the TSP signal over a short section covering the flawed region of the tube, and (c) the sizing results displayed in a separate window and with amplitude and depth profiles displayed in cross sectional plot and in image format. The results in this case indicate presence of a ~0.2-in.-long axial crack with a maximum depth of ~90% TW.



(a)

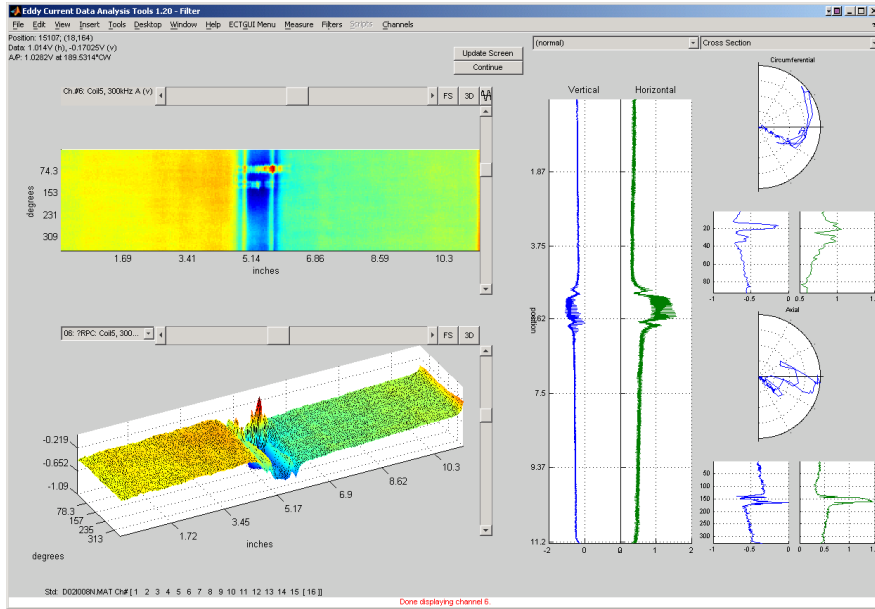


(b)

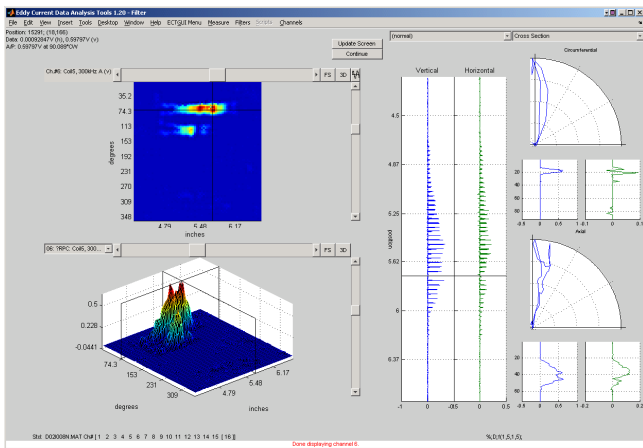


(c)

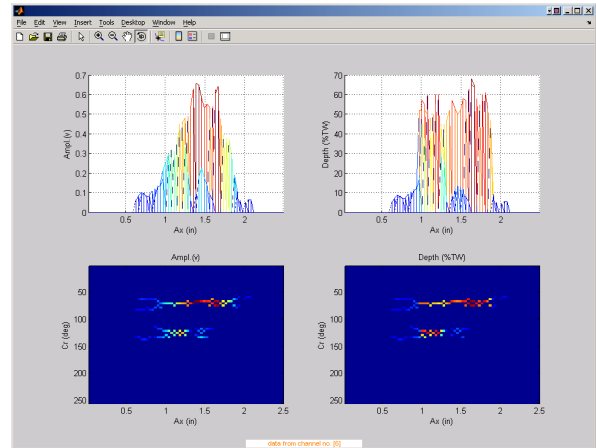
Figure 16. Display of data at various stages of the process for sizing of OD initiated circumferential indication in a mock-up tube section. Graphics show (a) the +Point™ data for the entire tube section at 300 kHz in various display formats, (b) filtered data over a short section covering the flawed region of the tube, and (c) the sizing results displayed in a separate window and with amplitude and depth profiles displayed in cross sectional plot and in image format. The results in this case indicate presence of >200° circumferential cracking with a maximum depth of ~70% TW.



(a)

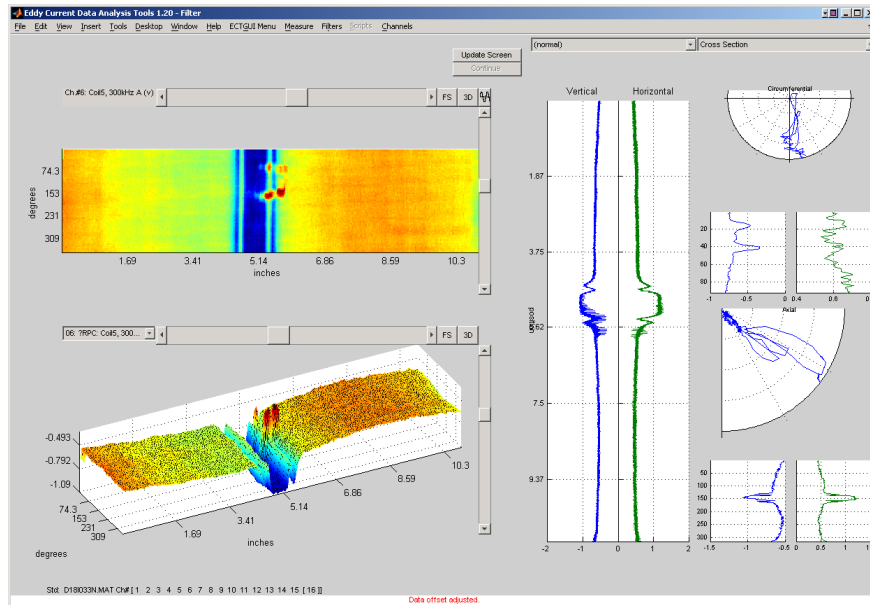


(b)

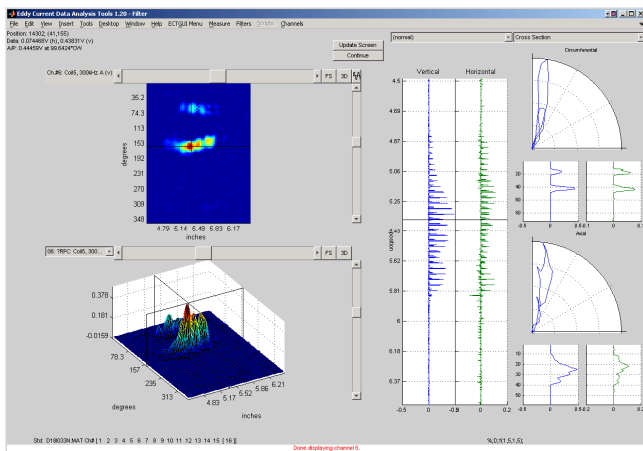


(c)

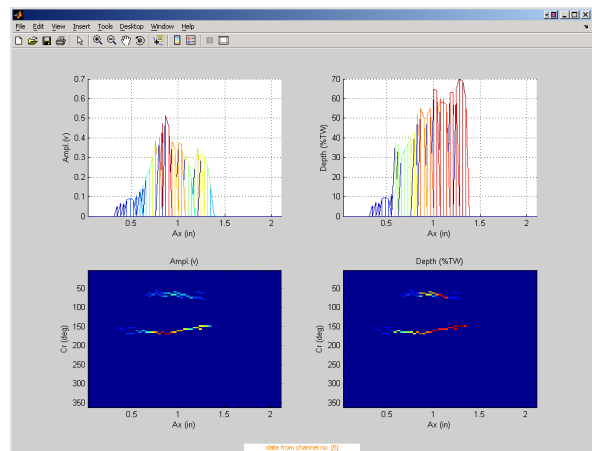
Figure 17. Data displayed at various stages of the process for sizing of indications at a dented TSP region in a mock-up tube section. Graphics show (a) the calibrated +Point™ data for the entire tube section at 300 kHz in various display formats, (b) filtered data over a short section covering the flawed region of the tube, and (c) the sizing results displayed in a separate window and with amplitude and depth profiles displayed in cross sectional plot and in image format. The results in this case indicate presence of multiple OD axial indications with the longer indication having a length of >1-in. with an average depth of ~60%TW and a maximum depth of <70% TW.



(a)

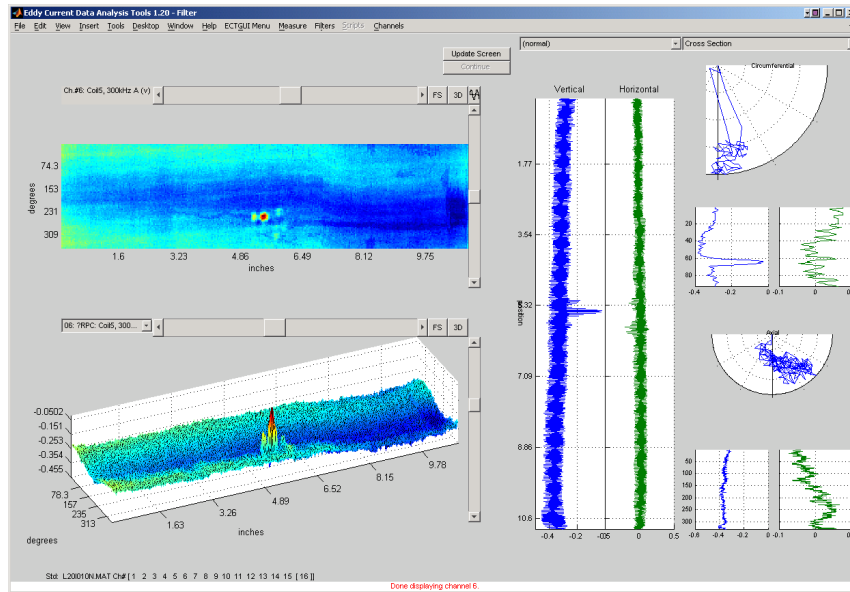


(b)

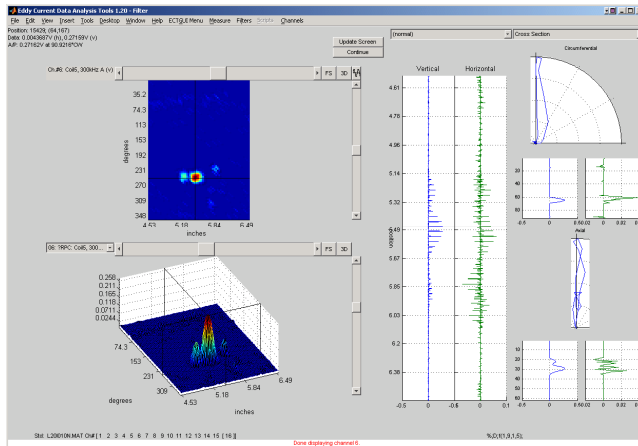


(c)

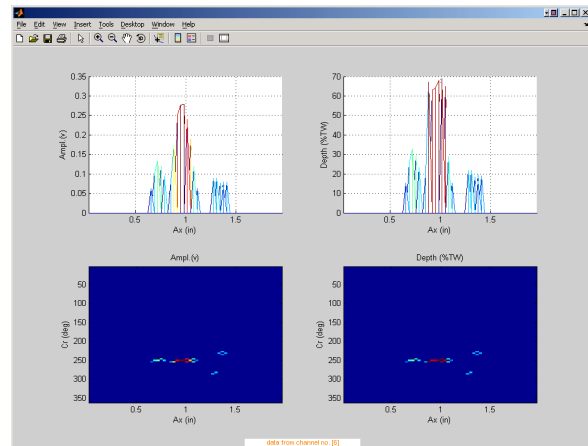
Figure 18. Data displayed at various stages of the process for sizing of indications at a dented TSP region in a mock-up tube section. Graphics show (a) the calibrated +Point™ data for the entire tube section at 300 kHz in various display formats, (b) filtered data over a short section covering the flawed region of the tube, and (c) the sizing results displayed in a separate window and with amplitude and depth profiles displayed in cross sectional plot and in image format. The results in this case indicate presence of multiple OD axial indications with the longer indication having a length of <1-in. and a maximum depth of ~70% TW.



(a)



(b)



(c)

Figure 19. Data displayed at various stages of the process for sizing of indications at a dented free-span region in a mock-up tube section. Graphics show (a) the calibrated +Point™ data for the entire tube section at 300 kHz in various display formats, (b) filtered data over a short section covering the flawed region of the tube, and (c) the sizing results displayed in a separate window and with amplitude and depth profiles displayed in cross sectional plot and in image format. The results in this case indicate presence of multiple OD axial indications with the longer indication having a length of >0.25-in. and a maximum depth of <70% TW.

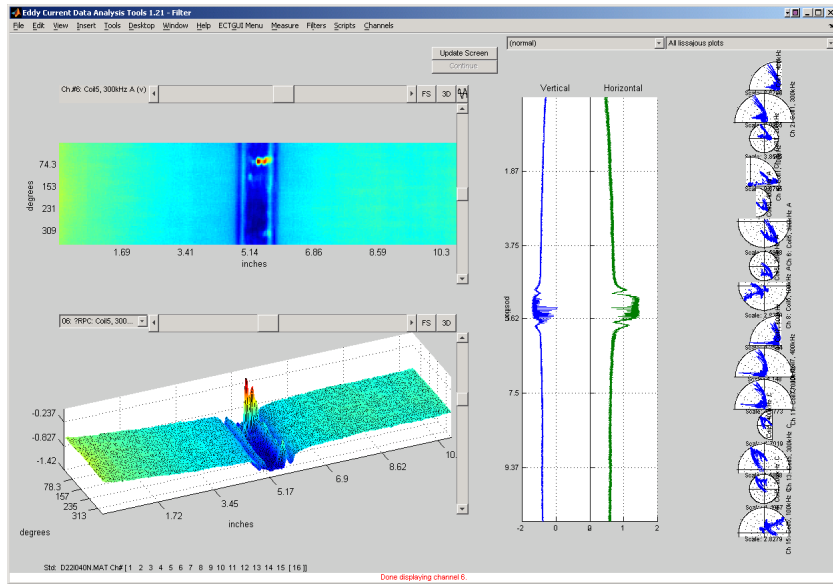
The data analysis results discussed so far were all based on sizing of flaws over a user-selected region of the tube. Examples are presented next on sizing of indications over the entire length of a mock-up tube section. As stated earlier, the available database of tubes used in this study generally contain single or multiple SCC indications over a localized area of the tube. To better evaluate the capability of the algorithms to detect and size multiple indications over the entire length of the tube, the data superposition tool under the GUI was used to simulate tubes with more than one flawed zone.

An example is presented next on sizing of indications over the entire length of tube based on rotating probe data. Figure 20(a) shows the data collected from a mockup tube section containing multiple indications at a dented TSP region. Figure 20(b) shows the same tube after superimposing the flaw signal, extracted from another tube, on three different locations over the tube. The same SCC signal was added to a free-span region and to two locations in the center and edge of the TSP. These three locations were selected to further examine the influence of background on the flaw signal. The +Point™ probe data displayed in Fig. 20(b) shows a smooth transition along the edges of the inserted signal at all three locations. Intermediate stages of the process for sizing of indications in the simulated tube section of Fig. 20 are displayed in Fig. 21. Fig. 21(a) shows the results following the pre-processing, detection and rule-based identification stage. The sizing result displayed by the GUI over the entire tube length is shown in Fig. 21(b). The data in this case indicates that in addition to the original signals in the TSP region of the tube, all three simulated flaw signals are also detected and sized. The amplitude and depth profile for the three superimposed signals is shown in Fig. 22. Data is displayed for small segments of the tube covering the flawed region. The graphics in Fig. 22 were generated in a separate window by using a plotting routine available under the measurement menu. Comparison of the amplitude and depth profiles of the same flaw signal added to three different locations suggests good agreement between the sizing results. The results in this case also indicate the effectiveness of the background suppression routines to both eliminate unwanted signals and to minimally perturb the flaw signal.

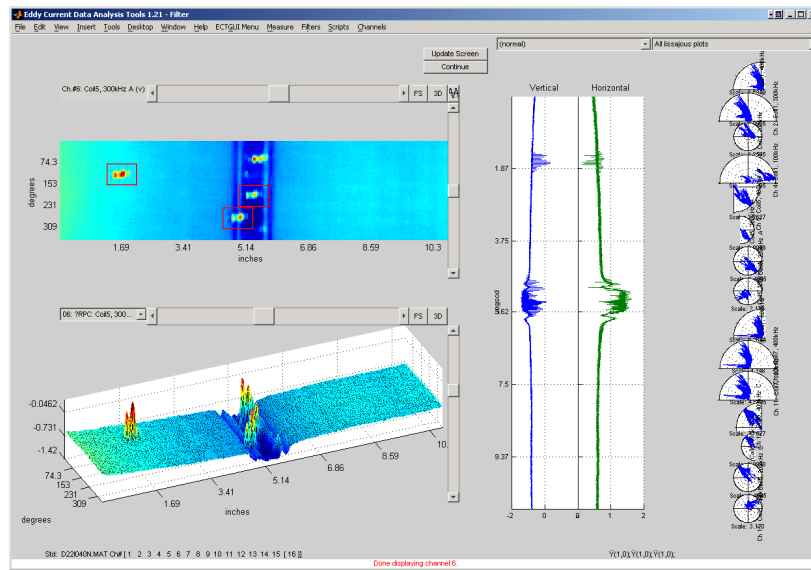
As described earlier, dynamic functions referred to here as *Depth Profilers* under the Filters menu of the GUI allow calculation of the flaw depth based on a number of different methods. These algorithms currently allow calculation of the flaw depth based on the available data from a single or multiple test frequencies. Alternate methods using the amplitude, phase, or the hybrid sizing can currently be applied. A representative test case is presented on comparison of flaw sizing results obtained using data from a single frequency with that obtained using multiple test frequencies.

Figure 23(a) shows the calibrated rotating probe data from the same mock-up tube section used in the previous example. The specimen was identified as having multiple SCC indications in conjunction with denting at the TSP region. The image and isometric plots displayed in the GUI window pertain to the 300 kHz channel of the +Point™ coil. The processed data following background suppression, detection, and identification of flaw signals is displayed in Fig. 23(b). The processed data at that stage suggest presence of multiple axial indications in the TSP region of the tube that consist of signals from a dominant flaw and two smaller flaws. Next, the flaw depths were estimated by using the phase angle information from the processed +Point™ data by employing one, two, and three test frequencies, respectively. Figure 24(a) displays the single-frequency sizing results for the same tube shown in Fig. 23. The calculated depth values over a small section of the tube containing the dominant flaw signal is shown in Fig. 24(b). For more quantitative comparison of the sizing results, the same data is displayed in Fig. 24(c). This separate graphics window was generated by using the display option available under the *Measure* menu. Both the amplitude and depth estimates are displayed in that panel in image format and as

isometric plots. The depth estimates for the same section of the tube based on the phase angle information from multiple channels are shown in Figs. 24(d) and (e). The sizing result in Fig. 24(d) was generated by using the data from 300 kHz and 400 kHz test frequencies. Figure 24(e) shows the sizing result based on the 200 kHz, 300 kHz, and 400 kHz test frequencies. Comparison of the depth profiles for the dominant flaw shown in Figs. 24(c)-(e) suggests good agreement among the three sizing methods. In all cases here, the flaw is predicted to have a maximum depth of slightly <90% TW. It should be noted, however, that more variation among the sizing results are expected for more complex flaws and for low-amplitude signals.

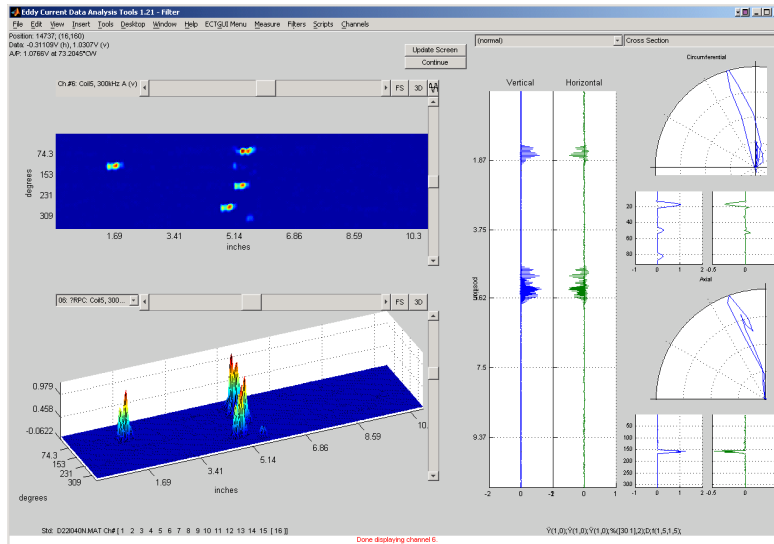


(a)

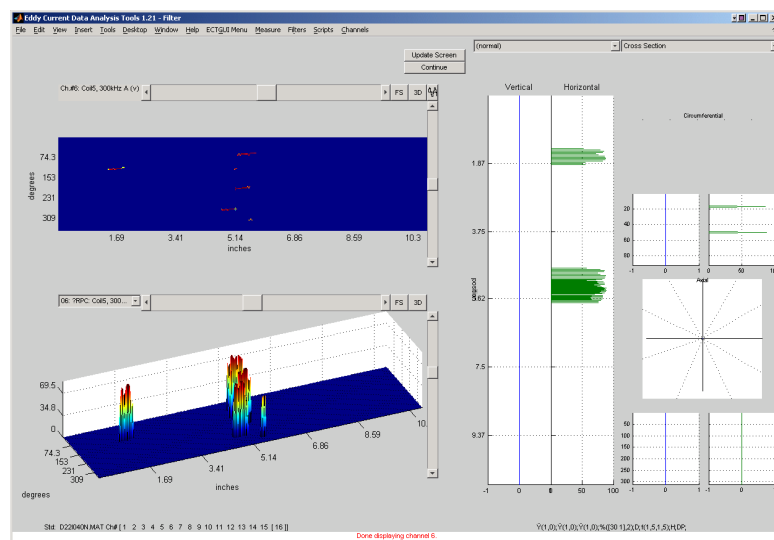


(b)

Figure 20. Example of superposition of EC inspection data collected from two separate tube sections. Simulated data here was generated to demonstrate sizing of indications over the entire length of tube. Graphics show (a) raw data from a tube section with multiple indications at a dented TSP region, and (b) the same tube with superimposed flaw signals. The same free-span SCC signal was inserted into three locations, one in the free-span region and two in the TSP region (center and edge), that are delineated on the image display. Eddy current inspection data displayed in the analysis window is from +Point™ probe at 300 kHz.

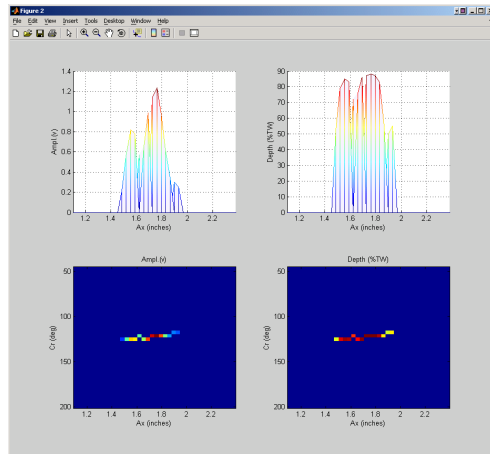


(a)

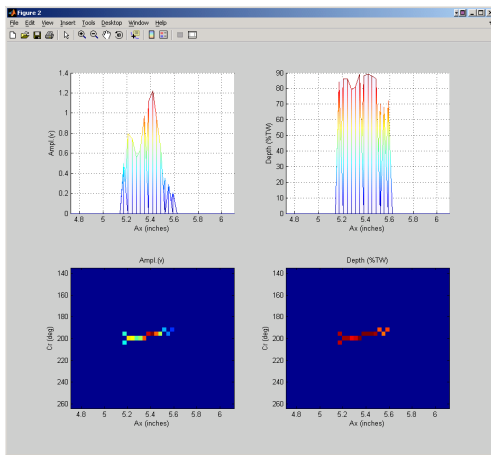


(b)

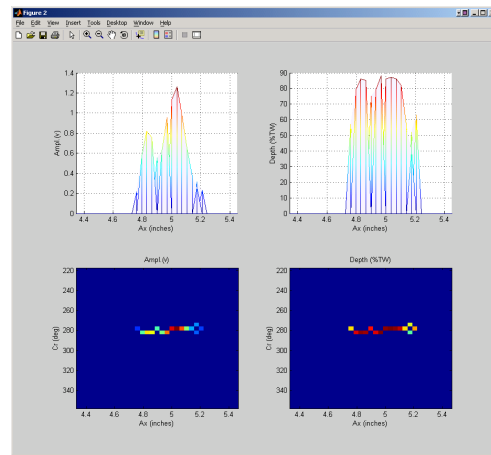
Figure 21. Data displayed at different stages of the process for sizing of indications in the simulated test section shown in Fig. 20(b). Graphics show (a) detected indications over the entire tube after elimination of background signals and (b) the depth sizing results over the entire length of the tube displayed in the main GUI. The results in this case indicate that in addition to the original signals in the TSP region of the tube, all three simulated flaw signals were also detected and sized.



(a)

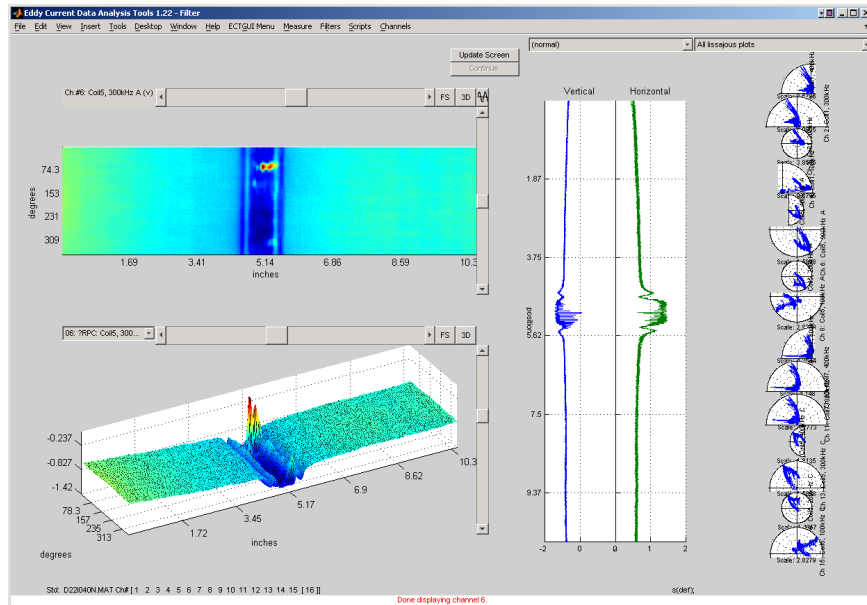


(b)

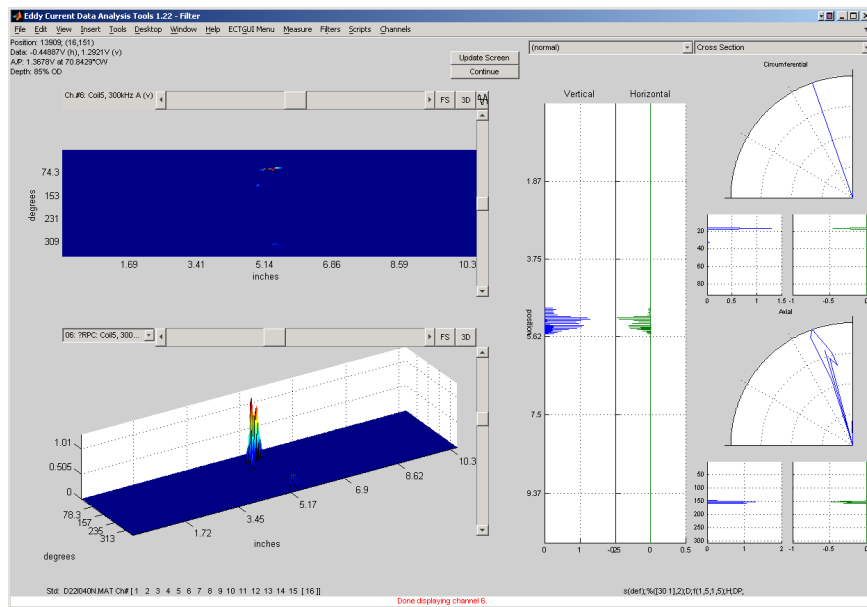


(c)

Figure 22. Data analysis results over three small segments covering the superimposed SCC signals of Fig. 21(b) located in free-span and TSP region of the tube. Graphics show the amplitude and depth profiles of the same indication based on the processed +Point™ data at the (a) free-span region, (b) center of TSP, and (c) the edge of TSP. The profiles for all three locations show good agreement among the sizing results.

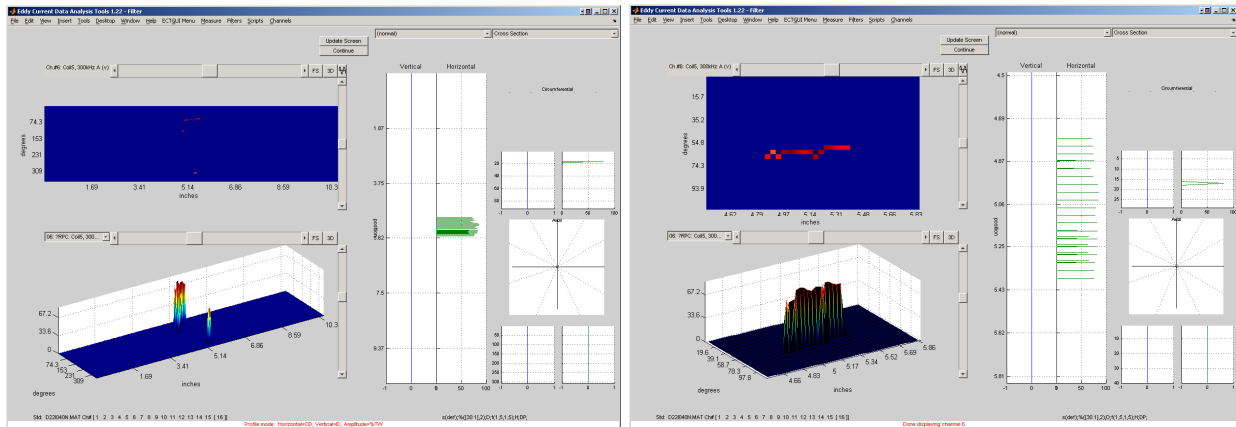


(a)



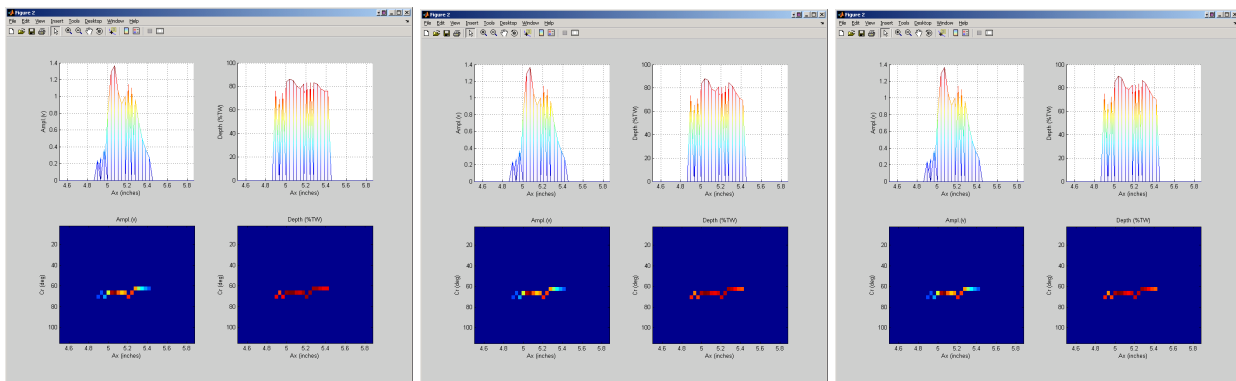
(b)

Figure 23. Display of the EC rotating probe data at different stages of the process for a tube section with multiple axial indications at a dented TSP region. Graphics show the +Point™ data at 300 kHz (a) after the calibration stage and (b) following the pre-processing, detection, and rule-based identification stage. The processed data suggest presence of multiple OD-initiated axial indications around the tube's circumference.



(a)

(b)



(c)

(d)

(e)

Figure 24. Flaw sizing results for the rotating probe data shown in Fig. 23. Shown here in the main GUI are the estimated depth values based on a single frequency (a) over the entire tube and (b) over a small region covering the dominant TSP indication. Also shown are the single and multiple frequency sizing data for the same region of the tube as in Fig. 24(b) using the phase information from (c) 300 kHz, (d) 400 and 300 kHz, and (e) 400, 300, and 200 kHz channels. The estimated depth profiles for the dominant flaw suggest close agreement between the three sizing results.

VI. Summary

An overview of research activities at Argonne associated with computer-aided analysis of EC inspection data was provided. The NDE results were used both to assess the capability of a particular EC inspection method for sizing of flaws and as input to mechanistic models for prediction of the structural integrity of SG tubes. The results of efforts on the development and integration of various algorithms for sizing of flaws based on eddy current rotating probe data have been discussed. The main focus of these investigations was on the processing of data acquired with the +Point™ probe, which is one of the more widely used probes for detection and characterization of cracking in SG tubes. It should be noted, however, that many of the processes described in this report are applicable to data acquired with other probe types. The overall structure of a software-based tool, developed under the MATLAB® environment, for the processing of data acquired with different EC probe types was described. The three main stages of the process that have been consolidated under a single graphical user interface are discussed. The main algorithms for sizing of flaws were also discussed. Representative cases have been provided on estimation of flaw size based on alternative methods. The examples demonstrate the options available for the processing of data over a selected region or the entire length of the tube. Other functions including those implemented for superposition of data and for exporting of data in standard formats were also described. It is worth noting that the data analysis tool developed under this program could be used to conveniently explore other potential approaches for improved characterization of flaws in SG tubes based on rotating probe data. A viable approach, not evaluated under this work, is to incorporate the available information from different coils of a multi-coil rotating probe. Eddy current inspection data from different coils could plausibly be used to implement more elaborate expert system algorithms for improved detection and in multivariate analysis routines for estimation of flaw depth.

References

1. S. Bakhtiari, D. S. Kupperman, and W. J. Shack, Assessment of Noise Level for Eddy Current Inspection of Steam Generator Tubes, NUREG/CR-XXXX (ANL-05/44), submitted for publication, Mar. 2008.
2. D. S. Kupperman, S. Bakhtiari, W. J. Shack, J. Y. Park, and S. Majumdar, "Evaluation of Eddy Current Reliability from Steam Generator Mock-Up Round-robin," NUREG/CR6785; ANL-01/22, Nov. 2001.
3. D. S. Kupperman, S. Bakhtiari, W. J. Shack, J. Y. Park, and S. Majumdar, "Eddy Current Reliability Results from the Steam Generator Mock-up Analysis Round-Robin: Revision 1," NUREG/CR-6791, 2008.
4. S. Bakhtiari and D. S. Kupperman, "Advanced NDE for Steam Generator Tubing," NUREG/CR-6638 (ANL-99/09), Jan. 2000.
5. S. Bakhtiari, J.Y. Park, D.S. Kupperman, S. Majumdar, and W, J, Shack, "Advanced Nondestructive Evaluation for Steam Generator Tubing," NUREG/CR-6746 (ANL-01/21), Sept. 2001.
6. S. Bakhtiari, J.Y. Park, D.S. Kupperman, S. Majumdar, and W. J. Shack, "Final Report on Advanced Nondestructive Evaluation for Steam Generator Tubing for the Second International Steam Generator Tube Integrity Program," NUREG/CR-6814 (ANL-03/4), July 2003.
7. D. S. Kupperman, J. Y. Park, S. Majumdar, S. Bakhtiari, K. Kasza and W. J. Shack, "Non-destructive and Failure Evaluation of Tubing from a Retired Steam Generator," NUREG/CR-6924, ANL-06/48, March 2007.
8. S. Majumdar, C.B. Bahn, Ken Kasza, and S. Bakhtiari, "Technical Letter Report on Validation of the Equivalent Rectangular Crack Method," NRC Letter Report, submitted for publication, Aug. 2008.